Bioactive Materials 17 (2022) 506–525

Contents lists available at ScienceDirect

Bioactive Materials

journal homepage: www.keaipublishing.com/en/journals/bioactive-materials

Significance of native PLGA nanoparticles in the treatment of Alzheimer's disease pathology

Bibin Anand [a,b,1], Qi Wu [a,b,1], Maryam Nakhaei-Nejad [a,1], Govindarajan Karthivashan [a,b,1], Lyudmyla Dorosh [c], Sara Amidian [b,d], Abhishek Dahal [b,e], Xiuju Li [a,b], Maria Stepanova [c], Holger Wille [b,d,e], Fabrizio Giuliani [a,e], Satyabrata Kar [a,b,e,*]

[a] Department of Medicine (Neurology), University of Alberta, Edmonton, Alberta, T6G 2M8, Canada
[b] Centre for Prions and Protein Folding Diseases, University of Alberta, Edmonton, Alberta, T6G 2M8, Canada
[c] Department of Electrical and Computer Engineering, University of Alberta, Edmonton, Alberta, T6G 2M8, Canada
[d] Department of Biochemistry, University of Alberta, Edmonton, Alberta, T6G 2M8, Canada
[e] Neuroscience and Mental Health Institute, University of Alberta, Edmonton, Alberta, T6G 2M8, Canada

ARTICLE INFO

Keywords:
Alzheimer's disease
β-amyloid
Nanoparticles
Neuroprotection
Peptide aggregation

ABSTRACT

Alzheimer's disease (AD) is believed to be triggered by increased levels/aggregation of β-amyloid (Aβ) peptides. At present, there is no effective disease-modifying treatment for AD. Here, we evaluated the therapeutic potential of FDA-approved native poly(D,L-lactide-*co*-glycolide) (PLGA) nanoparticles on Aβ aggregation and in cellular/animal models of AD. Our results showed that native PLGA can not only suppress the spontaneous aggregation but can also trigger disassembly of preformed Aβ aggregates. Spectroscopic studies, molecular dynamics simulations and biochemical analyses revealed that PLGA, by interacting with the hydrophobic domain of $A\beta_{1-42}$, prevents a conformational shift towards the β-sheet structure, thus precluding the formation and/or triggering disassembly of Aβ aggregates. PLGA-treated Aβ samples can enhance neuronal viability by reducing phosphorylation of tau protein and its associated signaling mechanisms. Administration of PLGA can interact with Aβ aggregates and attenuate memory deficits as well as Aβ levels/deposits in the 5xFAD mouse model of AD. PLGA can also protect iPSC-derived neurons from AD patients against Aβ toxicity by decreasing tau phosphorylation. These findings provide unambiguous evidence that native PLGA, by targeting different facets of the Aβ axis, can have beneficial effects in mouse neurons/animal models as well as on iPSC-derived AD neurons - thus signifying its unique therapeutic potential in the treatment of AD pathology.

1. Introduction

Alzheimer's disease (AD) is an unremitting neurodegenerative disorder characterized by a gradual loss of memory followed by deterioration of higher cognitive functions such as language, praxis and judgment [1,2]. Etiologically, most AD cases are sporadic, whereas only a minority (<10%) of cases segregate with mutations in three known genes: amyloid precursor protein (*APP*), presenilin 1 (*PSEN1*) and *PSEN2* [3,4]. The neuropathological features associated with AD include the presence of intracellular tau-positive neurofibrillary tangles, extracellular β-amyloid (Aβ)-containing neuritic plaques and the loss of neurons in defined brain regions [2,5]. Pathological changes that characterize AD, together with the constitutive production of Aβ in the normal brain, suggest that an overproduction and/or a lack of clearance may lead to increased Aβ levels which, in turn, contribute to neuronal loss and development of AD [1]. Although various Aβ fragments containing 39–43 amino acids are generated from APP by successive cleavage *via* the β-secretase and tetrameric γ-secretase complex, the two most prevalent isoforms found in the brain are $A\beta_{1-40}$ and $A\beta_{1-42}$ [1]. While $A\beta_{1-42}$ constitutes ~10% of the total Aβ peptide, it aggregates faster and is more toxic to neurons than the $A\beta_{1-40}$ isoform [6,7]. Conversion of Aβ from its soluble monomer into various aggregated states may underlie the cause of AD pathology as soluble oligomers and

Peer review under responsibility of KeAi Communications Co., Ltd.
* Corresponding author. Centre for Prions and Protein Folding Diseases, Department of Medicine (Neurology) and Psychiatry University of Alberta, Edmonton, Alberta, T6G 2M8, Canada.
E-mail address: skar@ualberta.ca (S. Kar).
[1] These authors contributed equally to this work.

https://doi.org/10.1016/j.bioactmat.2022.05.030
Received 18 November 2021; Received in revised form 26 April 2022; Accepted 23 May 2022
Available online 15 July 2022

Abbreviations

Aβ	amyloid β
AD	Alzheimer's disease
BBB	blood-brain barrier
APP	amyloid precursor protein
BCA	bicinchoninic acid
BDNF	brain-derived neurotrophic factor
CD	circular dichroism
CID	collision-induced dissociation
CSF	cerebrospinal fluid
CTF	c-terminal fragment
DLS	dynamic light scattering
DMEM	Dulbecco's modified Eagle's medium
DMSO	dimethyl sulfoxide;
ECL	enhanced chemiluminescence
ECD	essential collective dynamics
ERK1/2	extracellular signal-regulated kinases
FBS	fetal bovine serum
FDA	US Food and Drug Administration
FFR	field-free region
FTIR	Fouriertransform infrared spectroscopy
GDNF	glial-derived neurotrophic factor
GSK-3β	glycogen synthase kinase-3β
HBSS	Hanks' balanced salt solution
HFIP	hexafluoro-2-propanol
icv	intracerebroventricular
iPSC	induced pluripotent stem cells
ITC	isothermal titration calorimetry
LDH	lactate dehydrogenase
MAP	mitogen-activated protein
MAP2	microtubule-associated protein 2
MD	molecular dynamics
MI	memory index
MS	mass spectroscopy
MTT	3-(4,5-dimethylthiazolyl)-2,5-diphenyltetrazolium bromide
NeuN	neuronal nuclei
PAGE	polyacrylamide gel electrophoresis
PBS	phosphate-buffered saline
PFA	paraformaldehyde
PLGA	poly(D,L-lactide-co-glycolide)
SAD	sporadic AD
TEM	transmission electron microscopy
ThT	Thioflavin-T

protofibrils are the most toxic species rendering neurons vulnerable to dysfunction leading to death. Thus, preventing the aggregation of the Aβ monomer into toxic fragments is a promising strategy for averting/delaying the onset or arresting the progression of AD [8–10].

Over the last decade, nanoparticles, which are less than 100 nm in diameter with unique physio-chemical properties, have been explored extensively as an area of novel therapeutic modalities for the treatment of AD [11–13]. Acidic poly(D,L-lactide-*co*-glycolide) (PLGA) nanoparticles, which constitute a family of FDA-approved biodegradable polymers, have been studied primarily as vehicles for delivering drugs and other macromolecules to the target areas. In fact, PLGA is currently being used in the delivery of 15 FDA-approved drugs in a variety of conditions [11,14–16]. PLGA is synthesized from two different monomers, glycolic acid and lactic acid. Depending on the ratio of lactide to glycolide used for the polymerization, different forms of PLGA can be obtained, which are readily hydrolyzed in the body to produce the original monomers that serve as physiological byproducts of various metabolic pathways [14,16]. Recent studies have shown that PLGA-encapsulated or conjugated drugs/agents such as donepezil, memantine, curcumin, quercetin and selegiline can have beneficial effects on cellular and/or animal models of AD with satisfactory biocompatibility devoid of any toxicity [17–22]. However, apart from delivering drugs/agents, very little is known about the significance of native PLGA nanoparticles (i.e., PLGA without conjugation or encapsulation with any drug/agent) in relation to AD pathology. In this study, using a variety of experimental approaches, we showed that native PLGA can suppress spontaneous Aβ aggregation and trigger disassembly of aggregated Aβ fibers by interacting with its hydrophobic domain. We further showed that PLGA treatment not only protects mouse cortical cultured neurons against Aβ toxicity but also can mitigate AD-related pathology in the 5xFAD mouse model of AD. Finally, PLGA was able to attenuate Aβ-induced toxicity in cultured human neurons derived from induced pluripotent stem cells (iPSC) of AD patients, thus highlighting its unique untapped potential in the treatment of AD pathology.

2. Experimental

2.1. Materials

Dulbecco's modified Eagle's medium (DMEM), neurobasal medium, Hanks' balanced salt solution (HBSS), fetal bovine serum (FBS), Alexa Fluor 488/594 conjugated secondary antibodies, ProLong Gold anti-fade reagent, NuPAGE 4–12% Bis-Tris gels and ELISA kits for the detection of mouse and human $A\beta_{1-40}$ and $A\beta_{1-42}$ were purchased from R&D systems (Minneapolis, MN, USA). Neural Induction Medium (A1647801), B27, N2 and CultureOne Supplement were from Gibco, Thermo Fisher Scientific (Nepean, ON, Canada). The bicinchoninic acid (BCA) protein assay kit and enhanced chemiluminescence (ECL) kit were from Thermo Fisher Scientific, whereas LysoSensor Yellow/Blue DND-160 was from Invitrogen (Eugene, OR, USA). The ALZET® mini-osmotic pumps (Model 2004) and brain infusion kits were procured from DURECT Corporation (Cupertino, CA, USA). Isoforms of $A\beta_{1-42}$, $A\beta_{1-40}$, $A\beta_{17-42}$, $A\beta_{25-35}$ and the reverse sequence of $A\beta_{1-42}$ (i.e., $A\beta_{42-1}$) were purchased from R Peptide (Sunnyvale, CA, USA), whereas D23 N Iowa mutant $A\beta_{1-42}$ was procured from Ana Spec (Sunnyvale, CA, USA). Degradex® PLGA (50:50 resomer; mol. wt. 30000) and fluorescent Degradex® PLGA were obtained from Phosphorex (Hopkinton, MA, USA). The Degradex® PLGA (50:50 resomer) nanoparticles purchased from Phosphorex do not have any surfactants on the surface but contain ~6% mannitol as a cryoprotectant to prevent their aggregation during the lyophilization process. Additionally, native PLGA nanoparticles exhibit a polymer density of 1.3 g/cm^3 with a mean diameter of 0.1 μm. These nanoparticles, as recommended, were first dissolved in buffer, vortexed and then sonicated by using probe sonicator with 40 pulses and 40% amplitude to ensure that the nanoparticles are well suspended prior to use in various experimental paradigms. Hexafluoro-2-propanol (HFIP), Thioflavin-T (ThT), PLGA (50:50 and 75:25 resomers), mannitol, cerebrospinal fluid (CSF) and 3-(4,5-dimethylthiazol-2-yl)-2,5-diphenyltetrazolium bromide (MTT) were from Sigma-Aldrich (St. Louis, MO, USA). Brain-derived neurotrophic factor (BDNF) and glial-derived neurotrophic factor (GDNF) were from Peprotech (New Jersey, USA), the lactate dehydrogenase (LDH)-based cytotoxicity assay kit was from Promega (Wisconsin, USA) and the cell cytotoxicity assay kit was from Abcam (Cambridge, MA). Electron microscopy grids (Formvar/Carbon-

coated 200 mesh Copper grids) and uranyl acetate stain were purchased from TedPella (Redding, CA, USA). Sources of primary antibodies used in the study are listed in Table 1. All horseradish peroxidase-conjugated secondary antibodies were from Santa Cruz Biotechnology (Paso Robles, CA, USA). All other chemicals were obtained from either Sigma-Aldrich or Fisher Scientific.

2.2. Preparation of Aβ peptides

All lyophilized $A\beta_{1\text{-}42}$, $A\beta_{1\text{-}40}$, $A\beta_{17\text{-}42}$, $A\beta_{25\text{-}35}$, $A\beta_{42\text{-}1}$ and D23 N Iowa mutant $A\beta_{1\text{-}42}$ isoforms stored at −80 °C were first equilibrated at room temperature for 30min prior to dissolving in HFIP to obtain a 1 mM solution. Once dissolved, peptide aliquots were quickly dried using a SpeedVac to remove HFIP and then stored at −80 °C for subsequent use as described earlier [23]. In brief, prior to the experiments various isoforms of Aβ peptides were thawed at 4 °C, diluted first with dimethyl sulfoxide (DMSO) to 5 mM concentration and then with sterile dH_2O to 100 μM concentration. For the preparation of Aβ fibrils, diluted peptides were incubated at 37 °C overnight in phosphate-buffered saline (0.01 M PBS, pH 7.4), whereas for the oligomer formation, peptides were incubated at 4 °C in PBS overnight.

2.3. Thioflavin T (ThT) fluorescence assay

A universally used ThT fluorescent dye is utilized for detecting the amyloid fibril formation [24]. The aggregation kinetics of different concentrations (1–20 μM) of $A\beta_{1\text{-}42}$ were carried out at 37 °C for 24h in mimicked physiological conditions in 100 μL reaction buffer (10 mM Na_2HPO_4 with 40 mM NaCl; pH 7.4) in the presence or absence of 1–50 μM native PLGA. In parallel, ThT kinetic experiments were carried out with 10 μM $A\beta_{1\text{-}42}$ in the presence or absence 50 μM PLGA of different resomers (i.e., 50:50 and 75:25), 50 μM lactic acid, 50 μM glycolic acid or a mixture of 50 μM glycolic + lactic acid. Additionally, the effects of 50 μM PLGA on the aggregation of different Aβ isoforms ($A\beta_{1\text{-}40}$, $A\beta_{17\text{-}42}$, $A\beta_{25\text{-}35}$, D23 N Iowa mutant $A\beta_{1\text{-}42}$ and $A\beta_{42\text{-}1}$) were evaluated using ThT kinetics assays. The concentration of ThT was maintained at 30 μM throughout the experiment. For the disassembly experiments, the ThT signal was monitored for matured $A\beta_{1\text{-}42}$ aggregates with or without 2.5–50 μM PLGA over 120h. The fluorescence was measured every 15min, with excitation at 440 nm and emission at 480 nm with a cutoff filter at 475 nm using a FLUOstar omega BMG Labtech (Aylesbury, UK) or a Spectra max M5 (Molecular Devices, CA, USA). To validate that the effect is mediated by native PLGA and not mannitol that has been added as a cryoprotectant to prevent its aggregation, we performed two sets of experiment. In the first set, PLGA nanoparticles were dissolved in distilled water, centrifuged at 1000 rpm for 20min, washed three times, resuspended in PBS (0.01 M, pH 7.4) and then sonicated prior to performing ThT kinetic assays using 10 μM $A\beta_{1\text{-}42}$. In the second set, we performed a ThT kinetic assay with 10 μM $A\beta_{1\text{-}42}$ in presence or absence of 50 μM PLGA or 50 μM mannitol. All kinetics experiments were repeated nine times with three technical replicates for each sample and the data are presented as means ± SEM. The kinetic traces from various experiments were normalized and graphs were plotted as % of control using ORIGIN 2020 software. Along with kinetics, various Aβ samples (100 μl), after incubation with or without PLGA for different times (30min-120h), were transferred to a clean glass slides, air-dried, stained with ThT and then examined using a Nikon 90i fluorescence microscope at 20× magnification [25].

Table 1
Details of the primary antibodies used in this study.

Antibody Type	Type	WB/FT/IFC dilution	Source
Amyloid Fibrils OC	Polyclonal	1:1000	Sigma-Aldrich
APP (clone Y188)	Monoclonal	1:1000	Abcam
β-actin	Monoclonal	1:5000	Sigma-Aldrich
β-amyloid, 1–15 (3A1)	Monoclonal	1:1000	BioLegend
β-amyloid, 1–16 (6E10)	Monoclonal	1:1000	BioLegend
β-amyloid, 17–24 (4G8)	Monoclonal	1:1000	BioLegend
β-amyloid, 23-29	Polyclonal	1:1000	Anaspec
β-amyloid, 37-42	Polyclonal	1:1000	Antibodies-online
Cathepsin D	Polyclonal	1:200	Santa Cruz
Cleaved-Caspase-3	Monoclonal	1:1000	Cell Signaling
MAP2	Monoclonal	1:500	Invitrogen
NeuN	Monoclonal	1:300	Abcam
Phospho-ERK	Polyclonal	1:1000	Cell Signaling
Phospho-GSK	Polyclonal	1:1000	Abcam
PSD-95	Polyclonal	1:500	Abcam
SMI312	Monoclonal	1:500	Biolegend
Synapsin-1	Polyclonal	1:1000	Thermo Fisher
Total-ERK	Monoclonal	1:1000	Cell Signaling
Total-GSK	Monoclonal	1:1000	Abcam
Tau (AT270)	Monoclonal	1:1000	Thermo Fisher
βIII Tubulin	Polyclonal	1:1000	Millipore

WB: western blotting; FT: filter-trap assay; IFC: immunofluorescence.

2.4. Transmission electron microscopy (TEM)

Aggregates of 10 μM $A\beta_{1\text{-}42}$ collected from kinetic reaction at different times, native PLGA alone and 10 μM $A\beta_{1\text{-}42}$ aggregates in the presence or absence of 50 μM PLGA were placed on 200 mesh carbon-coated copper grids for ~2min followed by a series of washing with ammonium acetate buffer. The washed samples were negatively stained by 2% Na phosphotungstate (pH 7.2) for 10min, washed, dried and then examined using an accelerating voltage of 200 kV. The stained samples were analyzed with a FEI Tecnai G20 TEM and micrographs were recorded using an Eagle 4kx4k CCD camera (FEI Company).

2.5. Dynamic light scattering (DLS)

The surface charge and hydrodynamic radii of PLGA alone as well as 10 μM $A\beta_{1\text{-}42}$ with or without different concentrations (2.5–50 μM) of PLGA were measured using a Malvern Zetasizer-Nano ZS (Malvern Instruments, Massachusetts, USA) equipped with a back-scattering detector (173°). The nanoparticle samples were prepared by filtering them through a pre-rinsed 0.2 μm pore size filter and all readings were recorded after equilibrating the samples for 5min at 25 °C. Particle size was calculated by the manufacturer's software through the Stokes-Einstein equation, assuming spherical shapes of the particles [23].

2.6. Circular dichroism (CD) spectroscopy

The changes in the secondary structure of aggregated $A\beta_{1\text{-}42}$ were determined using a Chirascan qCD spectropolarimeter as described earlier [25]. After incubating $A\beta_{1\text{-}42}$ monomer/aggregate in the presence or absence of 50 μM PLGA, the reaction mixture was subjected to spectroscopic studies and the CD spectra were recorded at room temperature in a CD cuvette of 2 mm path length. The reported spectra were the average of 9 different acquisitions between 200 and 260 nm. The alteration in the secondary structure of $A\beta_{1\text{-}42}$ was determined by analyzing the ellipticity values of the samples taken from the aggregation reactions with or without PLGA using the online server BeSTSel.

2.7. Fourier-transform infrared (FTIR) spectroscopy

A FTIR spectroscopy study was performed to identify the secondary structural vibration of the aggregated 10 μM $A\beta_{1\text{-}42}$ in the presence or absence of 50 μM PLGA. ATR mode was used to obtain the secondary derivative (1700 cm^{-1} and 1600 cm^{-1}) spectra. All the spectra were taken from a Bruker Vertex 70 spectrometer equipped with a silicon carbide source and an MCT detector. The spectral readings were processed using OPUS 6.5 software as described earlier [26].

2.8. Isothermal titration calorimetry (ITC)

The thermodynamics of $A\beta_{1\text{-}42}$ and PLGA were studied using a Microcal ITC at 298K in a high feedback gain mode with a differential power of 10 μcal/s at 250 rpm [27]. In brief, 10 μM $A\beta_{1\text{-}42}$ was injected at a flow rate of 0.25 μl/min into the sample cell containing 600 μM PLGA. The reference cell was filled with degassed water. All samples were degassed at 4 °C before titration to prevent the possible formation of air bubbles in the sample cell. To correct for the heat of dilution, standard experiments were performed for PLGA with PBS, PBS alone and $A\beta_{1\text{-}42}$ in the presence or absence of PLGA. All data were analyzed and fitted for a single site of interaction with the inbuilt ORIGIN software.

2.9. Fluorescence quenching

The interaction between Aβ and PLGA was quantified by using fluorescence quenching experiments [26]. All samples were prepared in PBS and the interaction between $A\beta_{1\text{-}42}$ monomers, $A\beta_{1\text{-}42}$ fibers and fluorescent-labelled PLGA was recorded using a Spectra Max M5. The concentration of PLGA was kept constant at 2 μM, whereas the concentration of $A\beta_{1\text{-}42}$ was varied between 42 and 294 nM. For the quenching studies for $A\beta_{1\text{-}42}$ fibers with PLGA the concentration of 10 μM PLGA was selected with the varied concentrations (42–294 nM) of $A\beta_{1\text{-}42}$ fibers. The PLGA was excited at 440 nm and the slit width was fixed to 10 nm for excitation and emission. The emission spectra were collected from 450 to 650 nm at room temperature. Binding constants were calculated using fluorescence intensity values at the maximum emission of 500 nm. From these values, we calculated the Stern Volmer constant, predicted the nature of binding constant and the number of binding sites. The obtained fluorescence spectra for the PLGA were analyzed by using the Stern Volmer equation [28].

$$F_0/F = 1 + \tau_o\, k_q\, [Q] = 1 + K_{sv}\, [Q]$$

F_0 = Fluorescence intensity in the absence of quencher,
F = Fluorescence intensity in the presence of quencher, Q = Concentration of the quencher.

The data were plotted and the slope value of the linear fit Stern Volmer constant [K_{sv}] was determined. From this, it can be predicted if binding of PLGA with the $A\beta_{1\text{-}42}$ is static or dynamic using the formula $K_{sv} = \tau_o\, [k_q]$ where τ_o is the average life-time of any biomolecule. The binding site (n) and the binding constant (Ka) of $A\beta_{1\text{-}42}$ to PLGA were calculated by the formula:

$$\log\, [(F_0 - F)/F] = \log\, (Ka) + n\log\, [Q]$$

F_0 = Fluorescence intensity in the absence of quencher, F = Fluorescence intensity in the presence of quencher, Q = Concentration of the quencher, Ka = binding constant, n = number of binding sites. The values of log [$(F_0–F)/F$] were calculated and a graph was plotted against the calculated log [Q] values. A linear fit of the data was carried out to extract important parameters such as binding constant (Ka) and the number of binding sites (n).

2.10. Interaction of $A\beta_{1\text{-}42}$ with PLGA and epitope mapping

To determine if native PLGA can interact with $A\beta_{1\text{-}42}$ in presence of other proteins, we performed an experiment where black 96 well plates were coated with 10 μM $A\beta_{1\text{-}42}$ at 4 °C overnight and then exposed to 50 μM FITC-conjugated fluorescence PLGA dissolved in either human CSF or PBS for 4hr. After incubation, plates were washed and the fluorescence intensity was measured with excitation at 460 nm and emission at 500 nm using a Spectra max M5 (Molecular Devices, CA, USA). To detect the presence/absence of higher order Aβ entities after incubation of 10 μM $A\beta_{1\text{-}42}$ aggregates with or without 2.5–50 μM PLGA for 24–120h, we used native polyacrylamide gel electrophoresis (PAGE) as described earlier [25]. The Native PAGE was performed using a 12% polyacrylamide gel at 4 °C using an Invitrogen Novex mini cell system. The gels were then silver stained, visualized by a FluorChem E system (CA, USA) and the images were processed using Image J software. Subsequently, a filter-trap assay was used to determine the potential sites of interaction between $A\beta_{1\text{-}42}$ and PLGA using various site-specific Aβ antibodies (see enclosed Table 1) [27]. In a parallel set of experiments, different $A\beta_{1\text{-}42}$ conformers (monomers, oligomers and fibrillar) were incubated with 50 μM PLGA for 10min and then processed for the filter-trap assay using site-specific Aβ antibodies. In brief, various $A\beta_{1\text{-}42}$ samples with or without PLGA treatment were spotted on a nitrocellulose membrane (0.02 μm), subjected to vacuum filtration through a 96-well Bio-Dot Microfiltration system, washed with Tris-buffered saline and then incubated at 4 °C for 12h with aggregate specific anti-Aβ OC antibody as well as different sequence-specific Aβ antibodies. The membranes were further washed with buffers, incubated with appropriate horseradish peroxidase-conjugated secondary antibodies (1:1000) and developed with an ECL kit. All blots were examined using a FluorChem E system (Santa Clara, CA, USA) and the images were processed by using Image J software.

2.11. Molecular docking and post-docking simulations

Coordinates of the PLGA molecule from the PubChem database [29] (CID 23111554) were converted into PDB format (Discovery Studio software; Biovia 2016). To simplify the *in-silico* analyses, single PLGA molecules were used together with: monomeric $A\beta_{1\text{-}42}$ in water (Sup. Fig. S11A); a solution consisting of 8 monomers in water (Sup. Fig. S11B); an oligomeric system after aggregation (Sup. Fig. S11C) and a fibril fragment (Sup. Fig. S11D; Sup. Table S1). Initial coordinates of the $A\beta_{1\text{-}42}$ monomer were extracted from a 4 Å-resolution cryo-EM-based nonamer 5OQV [30]. Protonation states of Aβ peptides were modified to change the pH from the initial value of 2.0–7.4 using the PROPKA server [31] and the Gromacs 2018.7 [32] conversion script. Both C- and N-termini of Aβ were kept charged, while monomeric Aβ was minimized *in vacuo* and solvated. To neutralize the net charge, Na^+ counter ions were added and minimized with solvent, equilibrated and a representative conformation was selected using the UCSF Chimera software [33]. In order to obtain random conformations of monomers in solution, a 10ns molecular dynamics (MD) simulation was performed using Gromacs [32]. To prepare the solution, eight representative conformations from the 10ns trajectory were chosen by clustering using Chimera [33]. These peptides were placed at random positions at least 2.2 nm apart from each other and used as a model for subsequent solution simulations. In order to obtain an Aβ aggregate, the 8 chains were solvated and used for 100ns MD simulations using an isothermal-isobaric (NPT) ensemble. During MD simulations, the solution aggregated into a relatively compact octamer from which a representative snapshot was obtained by clustering using Chimera [33]. The octameric fibril fragment that remained after the removal of chain A from the 5OQV structure was used as an Aβ fibril with an exposed internal region. The resulting four representative Aβ systems (see Sup. Fig. S11; Sup. Table S1) including the monomer, the solution, the oligomer and the fibril fragment were used as templates for PLGA-Aβ docking using Autodock [34] implemented in Chimera [33]. For each system, the top ten docking models where PLGA occupies different binding sites were downloaded for subsequent analysis. If preferred docking sites coincided, we kept only the best-scored model, varying the number of bound PLGA molecules in different systems. The Aβ monomer contained four PLGA molecules, the solution of eight Aβ monomers six, the octamer seven and the fibril six, respectively. All systems were solvated, minimized and equilibrated.

2.12. Molecular dynamics (MD) simulations and analysis

We used Gromacs 2018.7 [32] to carry out all post-docking MD

simulations for 30–70ns. A specially designed OPLS-AA forcefield for PLGA molecules [35], a matching OPLS-AA forcefield for Aβ peptides [36] and an explicit SPC/E model for water [37] were employed. Additionally, a Verlet cut-off distance of 1.4 nm, V-rescale temperature coupling and Parrinello-Rahman pressure coupling were used for the minimization and equilibration []. The production simulations were carried at 310K temperature and 1atm pressure with isotropic pressure coupling (NPT ensemble) using an 1fs time step. For the identification of hydrogen bonds and inspection of PLGA orientation Chimera [33] was used. Snapshots from trajectories and graphical representation of the models were carried out using Chimera or Discovery Studio [33], whereas other plots were built with a gnuplot tool. In addition, we complemented these analysis tools with a new essential collective dynamics (ECD) analysis, which allows identification of efficiently stable dynamic coupling properties between atoms or atomic groups in a molecule from relatively short MD trajectories [38].

2.13. Mass spectroscopy (MS) analysis

To determine if 50 μM PLGA following 24–240h interaction with 10 μM $A\beta_{1-42}$ is hydrolyzed into glycolic and lactic acids, MS analysis of lactic acid, glycolic acid and PLGA with or without $A\beta_{1-42}$ was carried out using an Agilent 6220 tandem mass spectrometer equipped with a FAB gun that produces a 6 keV xenon beam (Santa Clara, CA, USA). Measurements were made in the negative-ion mode with glycerol as a matrix. The ion accelerating voltage was 10 kV and argon was used as collision gas. MS/MS spectra were obtained by performing collision-induced dissociation (CID) in the third field-free region (3rd FFR) between MS-1 and MS-2. In the case of MS/MS/MS (MS3), 1st generation production generated from the precursor ion by CID in the first FFR was introduced to the 3rd FFR where CID was further performed. To the collision cell located in the 3rd FFR, a voltage corresponding to 30% of the kinetic energy of the selected ion was passed through MS-1.

2.14. Mouse cortical neuronal cultures and treatments

Timed pregnant BALB/c mice purchased from Charles River (St. Constant, Quebec, Canada) were maintained according to Institutional and Canadian Council on Animal Care guidelines. Primary cortical cultures were prepared from 18-day-old embryos of timed pregnant mice as described previously [39,40]. In brief, the frontal cortex from pup brains was dissected in Hanks' balanced salt solution supplemented with 15 mM HEPES, 50 μM L-glutamine, 1 mM Na-pyruvate, 10units/mL penicillin and 10 μg/ml streptomycin and then digested with 0.25% trypsin-EDTA. The cell suspension was filtered through a cell strainer and plated (1.5×10^5 cells/cm^2) on either 96-well plates (for survival/death assay), 6-well plates (for biochemical analysis) or 8-well chamber slides (for LysoSensor DND-160 and cathepsin D labeling). The cultures were grown at 37 °C in a 5% CO_2 humidified atmosphere in Neurobasal medium supplemented with B27/N2, 50 μM L-glutamine, 1 mM Na-pyruvate, 15 mM HEPES, 10 units/ml penicillin, 10 μg/ml streptomycin and 1% FBS. The medium was replaced 1 day later without FBS and neurons are treated on day 6 after plating. In brief, cultured neurons were treated with oligomeric 1–10 μM $A\beta_{1-42}$ or 5–25 μM native PLGA alone for 24h. In a parallel set of experiments, cultured neurons were treated with 10 μM $A\beta_{1-42}$ after 24h incubation with or without 25–50 μM PLGA. Additionally, neurons were treated with preformed $A\beta_{1-42}$ aggregates incubated with or without 2.5–50 μM PLGA for either 24 or 120h. The control and treated cultured neurons were processed for cell viability/toxicity assays, immunocytochemistry, LysoSensor labeling or Western blotting after 24h and/or 100h exposure.

2.15. iPSC-derived AD neuronal cultures and treatment

Human iPSC-derived neurons from two healthy controls and two sporadic AD patients were used to examine the effects of native PLGA on Aβ levels and toxicity. Two sporadic AD (i.e., SAD1-3 and SAD2-3) and one healthy control (i.e., NDC1) iPSCs, purchased from WiCell Research Institute Inc (Wisconsin, USA), were previously generated and characterized [41]. One iPSC was derived from erythroid progenitor cells enriched from whole blood (Stemcell Technologies) of a healthy control (i.e., HC) using a CytoTune®-iPS 2.0 Sendai Reprogramming Kit (Invitrogen). All these cells were maintained according to guidelines approved by the University of Alberta Biomedical Ethics Committee.

To generate neurons, iPSCs were first differentiated to neural progenitor stem cells using neural induction medium according to manufacturer instructions. The cells were then characterized by the neural progenitor markers Nestin and Pax6 and the contaminant was removed based on the expression of CD44 and lack of CD184 [42]. After sorting, $CD184^+/CD44^-$ progenitor cells were allowed to recover and passaged on poly-ornithine and laminin (P + L)-coated dishes in neuron differentiating medium containing neurobasal medium supplemented with B27, N2, CultureOne, glutaMAX, penicillin/streptomycin, 20 ng/ml BDNF, 20 ng/ml GDNF, 50 μg/ml ascorbic acid and 1 μg/ml laminin. To this medium, 1 mM dibutyryl cyclic-AMP sodium salt was also added for the first 7 days of differentiation. Neurons were then passaged after 7–10 days by treating with 100 units/ml accutase containing DNase for 20min or until lifted. DMEM/F12 containing 4% bovine serum albumin was then added to neurons and passed through a 40 μm filter. Neurons were finally seeded (3×10^5 cells/cm^2), fixed in 4% paraformaldehyde (PFA) and immunostained using various neuronal markers (see enclosed Table 1). The iPSC-derived neurons from two controls and two sporadic AD cases were characterized without any treatment . In parallel, cultured iPSC-derived neurons were treated with or without 5 μM $A\beta_{1-42}$ after 24h incubation in the presence or absence of 50 μM PLGA. The control and treated cultured neurons were then processed for cell viability/toxicity assays, ELISA or Western blotting after 24h and/or 100h exposure.

2.16. Cytotoxicity assays

Neuronal viability following various experimental paradigms was analyzed using MTT, LDH or cell cytotoxicity assay kits [23,43]. For the MTT assay, control and Aβ-treated culture plates with or without PLGA were replaced with new media containing 0.5 mg/mL MTT and then incubated for 4h at 37 °C with 5% CO_2/95% air. The formazan was dissolved in DMSO and absorbance was measured at 570 nm with a microplate reader. To substantiate MTT data, control and Aβ-treated neurons with or without PLGA were processed for either the measurement of LDH activity in the conditioned medium or cell toxicity assay using the respective kits. The absorbance for LDH was measured at 490 nm, whereas for cellular cytotoxicity absorbance was measured at 570 nm and 605 nm with a Spectramax M5 spectrophotometer. All cell viability/toxicity experiments were repeated three to five times with three technical replicates.

2.17. Confocal microscopy with LysoSensor

Earlier studies reported that Aβ toxicity was, in part, mediated following breakdown of lysosomal integrity reflected by an alteration from an acidic to a basic pH environment [40]. To evaluate if PLGA treatment can protect neurons by restoring lysosomal pH integrity, cortical neurons after treatment with 10 μM $A\beta_{1-42}$ for 24h in the presence or absence of 25 μM PLGA were exposed to 5 μM LysoSensor DND-160 for 10min and the fluorescent signal was measured under a Zeiss confocal microscope at excitation and emission wave lengths of 329 and 440 nm, respectively.

2.18. Intracerebroventricular (icv) administration of PLGA into 5xFAD and control mice

To determine the therapeutic potential of native PLGA in attenuating

AD pathology and behavior, we used 5xFAD mice which co-express three APP (Swedish mutation: K670N, M671L; Florida mutation: I716V; London mutation: V717I) and two PS1 (M146L and L286V) FAD mutations and the age-matched non-Tg controls on C57BL/6J background. The phenotype and characteristic features of these 5xFAD mice have been described [40,44]. These mice were purchased from The Jackson Laboratory (Bar Harbor, ME, USA) and housed on a 12h light/dark cycle with access to food and water *ad libitum* in accordance with Canadian Council on Animal Care guidelines. Three-month old 5xFAD mice along with age-matched wild-type (WT) control mice (n = 8/group) were stereotaxically inserted with a microcannula into the right ventricle (−0.8 mm mid/lateral, −0.1 mm antero/posterior and −3.0 mm dorso/ventral from Bregma) under anesthesia and connected to a mini-osmotic infusion pump (Model 2004) implanted subcutaneously on the back of the mouse. The pump infused either artificial CSF or native PLGA dissolved in CSF (at a constant flow rate of 0.25 μL/h) into the lateral ventricular pocket for 28 days. On the basis of volume and rate of synthesis/renewal of the mouse CSF [45], these conditions result in a concentration of 25 μM PLGA in the mouse CSF at equilibrium. Animals were monitored on a daily basis over 28 days of treatment for signs of weight loss and abnormal behavior. After the treatment, animals were subjected to a novel-object recognition test and then euthanized by decapitation or fixed by perfusion in 4% PFA for subsequent analysis. In a parallel study, to define if native PLGA can interact with brain Aβ deposition, 5xFAD (n = 3/group) and WT control (n = 3/group) mice were stereotaxically (−0.2 mm mid/lateral, −1.6 mm antero/posterior and −1.2 mm dorso/ventral from Bregma) injected with 5 μl fluorescent labelled native PLGA (25 μM) using a Hamilton syringe under anesthesia [46]. After 2h post-injection, the mice were fixed in 4% PFA by perfusion and processed for immunohistochemistry using aggregate specific OC Aβ antibody.

2.19. Western blotting

Western blotting was carried out on samples collected from CSF- and PLGA-treated 5xFAD and WT mice as well as on control and Aβ-treated cultured cells as described earlier [39,47]. In brief, brain tissues (parietal cortex and cerebellum)/cultured neurons were first homogenized with radioimmunoprecipitation lysis buffer and proteins were quantified using a BCA kit. Denatured samples were resolved on 10% polyacrylamide or 4–12% NuPAGE Bis-Tris gels, transferred to PVDF membranes, blocked with 5% milk and incubated overnight at 4 °C with various primary antibodies at dilutions listed in Table 1. The membranes were then incubated with appropriate horseradish peroxidase-conjugated secondary antibodies (1:5000) and immunoreactive proteins were detected with an ECL kit. All blots were re-probed with anti-β-actin antibody and quantified using Image J as described earlier [47].

2.20. Immunostaining and quantification

Fixed brain sections (20 μm; parietal cortex and cerebellum) from CSF and PLGA-treated 5xFAD and WT mice as well as cultured neurons were incubated overnight at 4 °C with various antibodies (see enclosed Table 1) and then processed as for immunostaining as described earlier [48]. In parallel, brain sections (3–5 sections/mouse) immunostained with anti-Aβ OC antibody were processed to quantify plaque load in both CSF- and PLGA-treated 5xFAD mice (n = 3/group) as described earlier [49]. Immunostained sections/cells were visualized using a Nikon Eclipse 90i fluorescence microscope with a Retiga 2000R Q imaging system (Nikon Instruments Inc., NY, USA) or with a Zeiss multiphoton confocal laser scanning microscope (LSM700, Carl Zeiss, Inc.).

2.21. ELISA for Aβ1-40 and Aβ1-42

$A\beta_{1\text{-}40}$ and $A\beta_{1\text{-}42}$ levels in the parietal cortex and cerebellum of 5xFAD and WT control mice (4–6 mice/group) treated with CSF or PLGA, and iPSC-derived cultured neurons from control and sporadic AD patients were measured using commercially available ELISA kits as described before [48]. For Aβ in conditioned media, iPSC-derived neurons after differentiation were incubated for 24h in serum-free Opti--MEM I and subsequently processed to measure human $A\beta_{1\text{-}40}/A\beta_{1\text{-}42}$ levels using ELISA kit. All samples were assayed in duplicate and each experiment was repeated 3 times.

2.22. Novel-object recognition test

The 5xFAD and WT control mice following 28 days administration of CSF or PLGA using mini-osmotic pumps were subjected to a novel-object recognition/memory test as described earlier [50]. In brief, on day one, mice were habituated for 5min in an open field empty box followed by a day two familiarization phase, where the mice were exposed to two different objects (10min) placed in the box. On day three, among the two objects, one of the objects was replaced with a novel object and the exploratory behavior of the mice towards the familiar and novel objects was quantified using a memory index, wherein "t_o" represents time exploring an object during the original exposure and "t_n" represents time spent exploring an object that is novel on re-exposure; memory index = $(t_n - t_o)/(t_n + t_o)$. In parallel, the total number of visits to the novel object for all animals were evaluated.

2.23. Statistical analysis

All data collected from a minimum of 3–6 biological repeats with each experiment performed in three replicates were expressed as means ± SEM. The cell viability data from cultured neurons were analyzed by one-way ANOVA followed by Bonferroni's *post-hoc* analysis for multiple comparisons with a significance threshold set at $p < 0.05$. *P* values indicate the following significances: *, $p < 0.05$; **, $p < 0.01$ and ***, $p < 0.001$. All statistical analysis was performed using GraphPad Prism (GraphPad Software, Inc., CA, USA).

3. Results

3.1. Characterization of spontaneous Aβ1-42 aggregation

Formation of Aβ fibrils, which are aggregates with repetitive cross-beta sheets stabilized by different molecular interactions, is a key event in AD pathogenesis [51,52]. ThT is a classic amyloid dye routinely used in detecting Aβ fibril formation due to its strong fluorescence emission upon binding to cross-β fibril structures [53]. Our aggregation kinetic studies revealed that 1–20 μM $A\beta_{1\text{-}42}$ dose-dependently increased peptide aggregation over 6h and then reached a plateau as indicated by enhanced ThT levels (Fig. 1A). The propensity of Aβ aggregation was validated by fluorescence imaging following ThT labeling (Fig. 1B) as well as TEM images revealing the presence of smaller protofibrils at 8h and large twisted fibrils at 24h (Fig. 1C). The conversion of $A\beta_{1\text{-}42}$ from its monomeric to fibrillar state evaluated by DLS displayed a change in $A\beta_{1\text{-}42}$ hydrodynamic radius from ~10 to 100 nm to ~100–10,000 nm over 24h incubation, indicating the formation of higher-ordered entities (Fig. 1D and E) with a Zeta potential of −32mV (Fig. 1F). Native-PAGE analysis also showed the presence of higher-ordered $A\beta_{1\text{-}42}$ aggregates following 24h incubation (Fig. 1G). CD spectroscopy further revealed that $A\beta_{1\text{-}42}$ monomers remained as an unstructured random coil with a negative peak around 195 nm as reported in a previous study [26]. Once the Aβ samples aggregate and form higher-ordered structures over 24h, the respective CD spectra showed the conformational switch towards β-sheet structure by giving a signature signal at 218 nm (Fig. 1H). Our FTIR analysis also showed that secondary derivate spectra generated through the ATR mode depicted characteristic vibrations at 1617, 1631, 1647, 1667 and 1686 cm^{-1} indicating the presence of β-sheet-enriched structures in $A\beta_{1\text{-}42}$ aggregates (Fig. 1I) [24].

Figure - 1

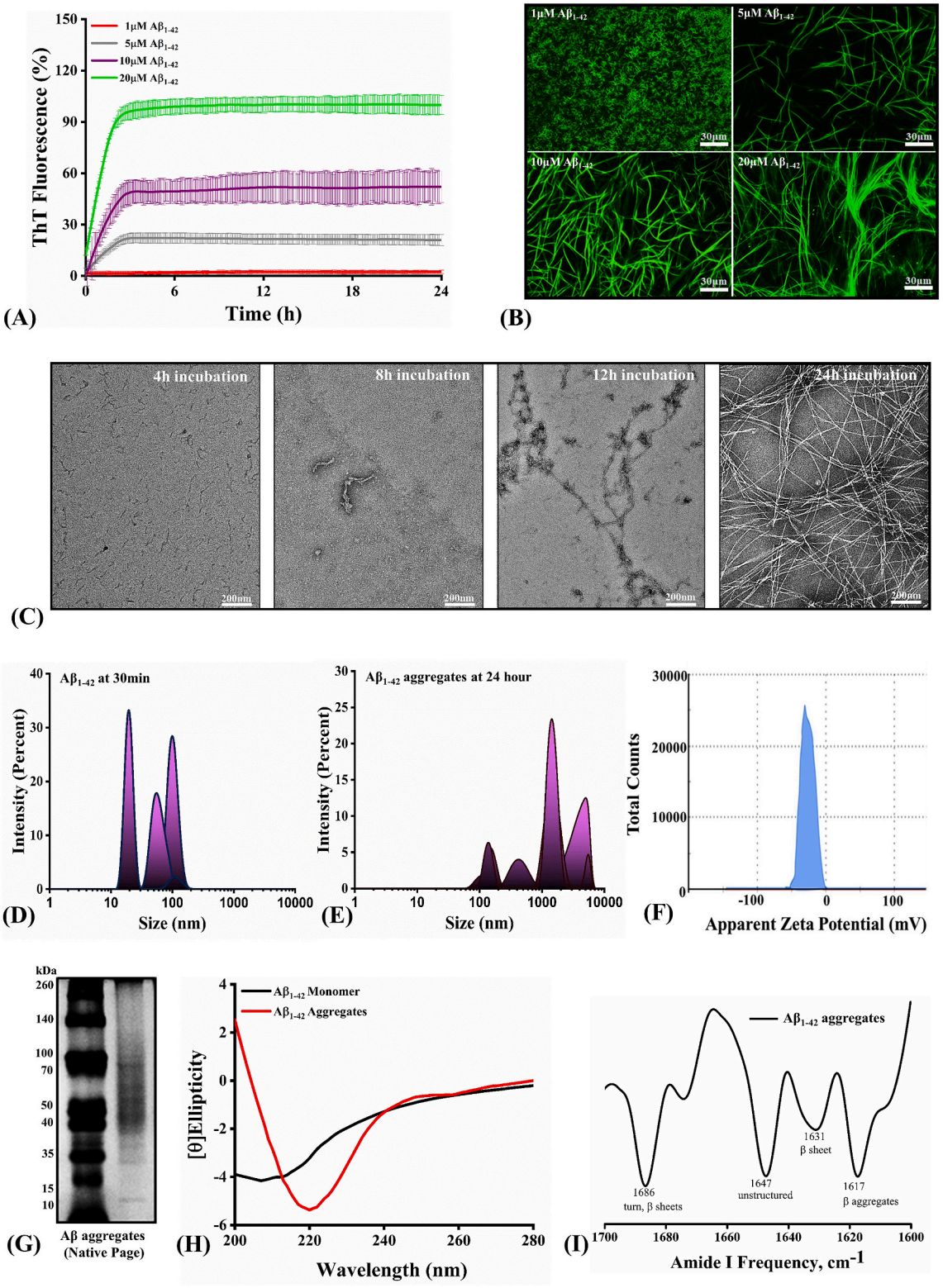

Fig. 1. Characterization of spontaneous $A\beta_{1-42}$ aggregation A; ThT assay revealing the dose-dependent (1–20 μM) spontaneous aggregation curves of $A\beta_{1-42}$ over 24h. Note the increased aggregation of $A\beta_{1-42}$ which reaches a plateau as indicated by ThT levels. **B;** ThT-stained fluorescence images depicting a dose-dependent (1, 5, 10 and 20 μM) increase in $A\beta_{1-42}$ aggregates after 24h. **C;** Time-dependent TEM micrographs showing the aggregation of $A\beta_{1-42}$ leading to the formation of matured fibers over 24h. **D & E;** DLS data revealing the hydrodynamic radius of monomeric and aggregated $A\beta_{1-42}$. **F;** Zeta potential measurement for $A\beta_{1-42}$ displaying surface charge of −32mV. **G;** Native PAGE of $A\beta_{1-42}$ aggregates showing the presence of higher ordered fibrillar entities after 24h. **H;** CD spectra for $A\beta_{1-42}$ monomers as well as aggregates confirming the formation of beta-sheet following aggregation of the peptide. **I;** FTIR secondary derivative spectra showing structural conformation $A\beta_{1-42}$ after aggregation.

3.2. Attenuation of Aβ1-42 aggregation by PLGA

Native PLGA nanoparticles, as observed in TEM, are mostly homogeneous with spheroidal morphology with an average diameter of ~100 nm (Fig. 2A and B). DLS analysis showed that PLGA nanoparticles are quite stable over a 240h period, with hydrodynamic radii of ~100 nm (Fig. 2C; Sup. Fig. S1) and a Zeta potential of ~8 mV (Fig. 2D). Subsequently, we evaluated the aggregation kinetics of 10 μM $A\beta_{1\text{-}42}$ in the presence or absence of 1–50 μM native PLGA over a 24h period at 37 °C using the ThT assay. Our data indicate that PLGA inhibited spontaneous $A\beta_{1\text{-}42}$ aggregation in a dose-dependent manner (Fig. 2E and F) which is validated by fluorescence imaging (Fig. 2G). Our TEM analysis revealed that PLGA nanoparticles, associated directly with Aβ fibers, attenuated peptide aggregation, leading to the formation of a heterogeneous mixture of smaller $A\beta_{1\text{-}42}$ aggregates (Fig. 2H). Suppression of Aβ aggregation was evident in DLS, native-PAGE analysis (Fig. 2I–K) and in our filter-trap assay with a fibril-specific OC antibody which showed decreased formation of $A\beta_{1\text{-}42}$ fibers in presence of PLGA (Fig. 2K, inset). CD spectroscopy revealed an increase in the helical content from 2.3 to 6.6% and a decrease in the β-sheet content from 38.6 to 28.8% in $A\beta_{1\text{-}42}$ samples treated with PLGA, suggesting an attenuation of the conformational transition of $A\beta_{1\text{-}42}$ from random coils to the β-sheets (Fig. 3A). Likewise, FTIR data showed the vibration of a 3_{10} α-helix and random coils in the presence of PLGA rather than the β-sheet-enriched structures observed in $A\beta_{1\text{-}42}$ aggregates, implying retention of the monomeric state (Fig. 3B). The inhibitory effects of 25 and 50 μM PLGA evaluated using ThT kinetic and fluorescence imaging over 24h with increasing concentrations (1–20 μM) of $A\beta_{1\text{-}42}$ also revealed an attenuation of Aβ aggregation over time (Sup. Figs. S2 and S3).

3.3. Specificity of PLGA-mediated inhibition of Aβ aggregation

Our kinetic data and fluorescence imaging of ThT assay samples showed that PLGA, as observed with $A\beta_{1\text{-}42}$, can suppress aggregation of 10 μM $A\beta_{1\text{-}40}$, $A\beta_{17\text{-}42}$ and $A\beta_{25\text{-}35}$ peptides (Sup. Fig. S4A–I). In parallel, PLGA can decrease aggregation of 10 μM familial D23N Iowa mutant $A\beta_{1\text{-}42}$, which is known to aggregate faster and to be more toxic to neurons than normal $A\beta_{1\text{-}42}$ [54], suggesting PLGA may be beneficial for sporadic as well as certain familial AD cases (Sup. Fig. S4J-L). Interestingly, 10 μM $A\beta_{42\text{-}1}$ (i.e., a negative control), which did not follow the aggregation kinetics of normal $A\beta_{1\text{-}42}$, was not affected by PLGA (Sup. Fig. S4M − O).

To establish the specificity of PLGA's effect, we showed that PLGA with 50:50 resomer from another source (i.e., Sigma-Aldrich) can suppress $A\beta_{1\text{-}42}$ aggregation, whereas equimolar PLGA with a 75:25 resomer composition did not alter Aβ aggregation (Fig. 3C). In parallel, $A\beta_{1\text{-}42}$ aggregation, as detected by the ThT kinetic assay, was not inhibited by either 50 μM lactic acid, 50 μM glycolic acid or a mixture of 50 μM lactic acid and glycolic acid (Fig. 3D). We further revealed that native-PLGA after washing to remove mannitol, which was added as a cryoprotectant, did suppress spontaneous Aβ aggregation (Sup. Fig. 5A). Additionally, 50 μM mannitol itself was unable to alter aggregation kinetics of $A\beta_{1\text{-}42}$ (Sup. Fig. 5B and C). To define if native PLGA can interact with $A\beta_{1\text{-}42}$ in the presence of other proteins, we evaluated the interaction of 10 μM $A\beta_{1\text{-}42}$ with 50 μM fluorescently labelled PLGA dissolved in either CSF or PBS. Our results clearly showed that fluorescently labelled native-PLGA can interact with $A\beta_{1\text{-}42}$ both in the presence of PBS and human CSF but the interaction is somewhat greater in presence of PBS compared to CSF (Sup. Fig. 5D), raising the possibility that native-PLGA in addition to Aβ may also interact with other proteins present in CSF. To determine if PLGA following interaction with Aβ is depolymerized into monomers we carried out a mass spectroscopic analysis to show that 50 μM PLGA following 120h and 240h incubation, but not after 24h incubation, with 10 μM $A\beta_{1\text{-}42}$ is depolymerized into glycolic acid, lactic acid and dimers of lactic acid (Sup. Figs. S6–S8).

3.4. Molecular interaction of PLGA with Aβ1-42

Our ITC experiments involving titration of PLGA to $A\beta_{1\text{-}42}$ showed an exothermic interaction with a Kd = $7.76\text{x}10^{-5}$M, a Ka = $1.286\text{x}10^{4}$ M^{-1} and a stoichiometry of ~1 (n = 0.519). The Gibbs free energy ΔG was found to be −10.52 kcal M^{-1} with an Enthalpy (ΔH) = −8.067 kcal M^{-1} and an Entropy (ΔS) = −8.256 kcal.$M^{-1}K^{-1}$ (Fig. 3E). In parallel, the fluorescence quenching revealed that the intrinsic fluorescence emission from PLGA was effectively quenched in a dose-dependent manner in the presence of monomeric $A\beta_{1\text{-}42}$, predicting a single binding site (n = 0.8) with a Kd of 9.09×10^{4} M for interactions between PLGA and Aβ (Fig. 3F; Sup. Fig. S9A and B). To define further the interface between Aβ and PLGA, $A\beta_{1\text{-}42}$ aggregates with or without PLGA were adsorbed onto nitrocellulose membranes (filter trap assay) and probed with various site-specific Aβ antibodies (Fig. 3G). The antibodies interacting with the Lsy_{17} and Ala_{42} regions of Aβ did not interact with PLGA-treated Aβ samples. Native PLGA also interacted with different $A\beta_{1\text{-}42}$ conformers (i.e, monomeric, fibrillar and oligomeric) following 10min exposure, but its binding to Aβ monomers was somewhat more site-specific than with Aβ oligomers or aggregates (Fig. 3H).

3.5. Disassembly of aggregated Aβ1-42 fibers by PLGA

To evaluate the therapeutic potential of PLGA in AD pathology, we incubated preformed $A\beta_{1\text{-}42}$ fibers with 2.5–50 μM native PLGA over 120h at 37 °C. Our ThT kinetic assay and fluorescence imaging studies revealed that PLGA can dose-dependently trigger the disassembly of matured $A\beta_{1\text{-}42}$ fibers into small fibrillar entities possibly due to disruption of β-sheet structure or interaction with the steric zippers present in $A\beta_{1\text{-}42}$ fibers (Fig. 4A–D; Sup. Fig. S10). This is supported by TEM data demonstrating the presence of PLGA nanoparticles in close contact with Aβ fibrils (Fig. 4E). Dismantling of PLGA-treated $A\beta_{1\text{-}42}$ fibers is also apparent by DLS (Fig. 4F–I) and native-PAGE (Fig. 4J), indicating the loss of higher-ordered $A\beta_{1\text{-}42}$ aggregates. Additionally, the fluorescence quenching effect of labelled PLGA in the presence of increasing concentrations of matured $A\beta_{1\text{-}42}$ fibers showed a dose-dependent decrease in fluorescence intensity, indicating a direct interaction between PLGA and $A\beta_{1\text{-}42}$ fibers that may underlie the unzipping of the steric zippers in the matured $A\beta_{1\text{-}42}$ fibers, yielding smaller fragments. The analysis of quenching data predicted a single binding site (n = 1.05) with a Kd value of 6.95×10^{7} M (Fig. 4K; Sup. Fig. S9C and D).

3.6. In-silico docking and MD simulations

To assess details of the PLGA interaction with various $A\beta_{1\text{-}42}$ constructs, we used *in-silico* docking combined with MD simulations and a monomeric, randomly shaped $A\beta_{1\text{-}42}$ peptide, a solution of monomeric Aβ chains, an Aβ oligomer or a fibril fragment as well as monomeric PLGA molecules (Sup. Table S1). Following docking of PLGA molecules onto each of the four Aβ systems (Sup. Fig. S11), the systems were solvated, equilibrated and post-docking MD simulations were performed. Conformations of the four systems after the production MD simulations are presented in Fig. 5A–D, and additional structural information is shown in Sup. Fig. S12. Some of the PLGA molecules detached in the course of equilibrations and MD simulations, but re-binding was observed (see Videos S1–S4). The buildup of hydrogen bonds was analyzed immediately after docking and post-docking MD simulations (Fig. 5A–D; Sup. Table S2). The analysis revealed a variety of binding sites for different systems (*e.g.*, residues Y10-E11-V12-H13, V18–F19–F20-A21-E22-D23, N-terminal residues E3, H6 and S8 and C-terminal residues A30-I31-I32, M35). Structurally, both lactic and glycolic groups of PLGA were involved in the binding, with slight preference for lactic acid (13 *vs.* 9 bonds). The binding of PLGA to the fibril fragment is distinct from other systems as the binding sites are limited to mainly central parts of Aβ peptides. In contrast, in the oligomeric system more than half of the binding sites involve the peptides'

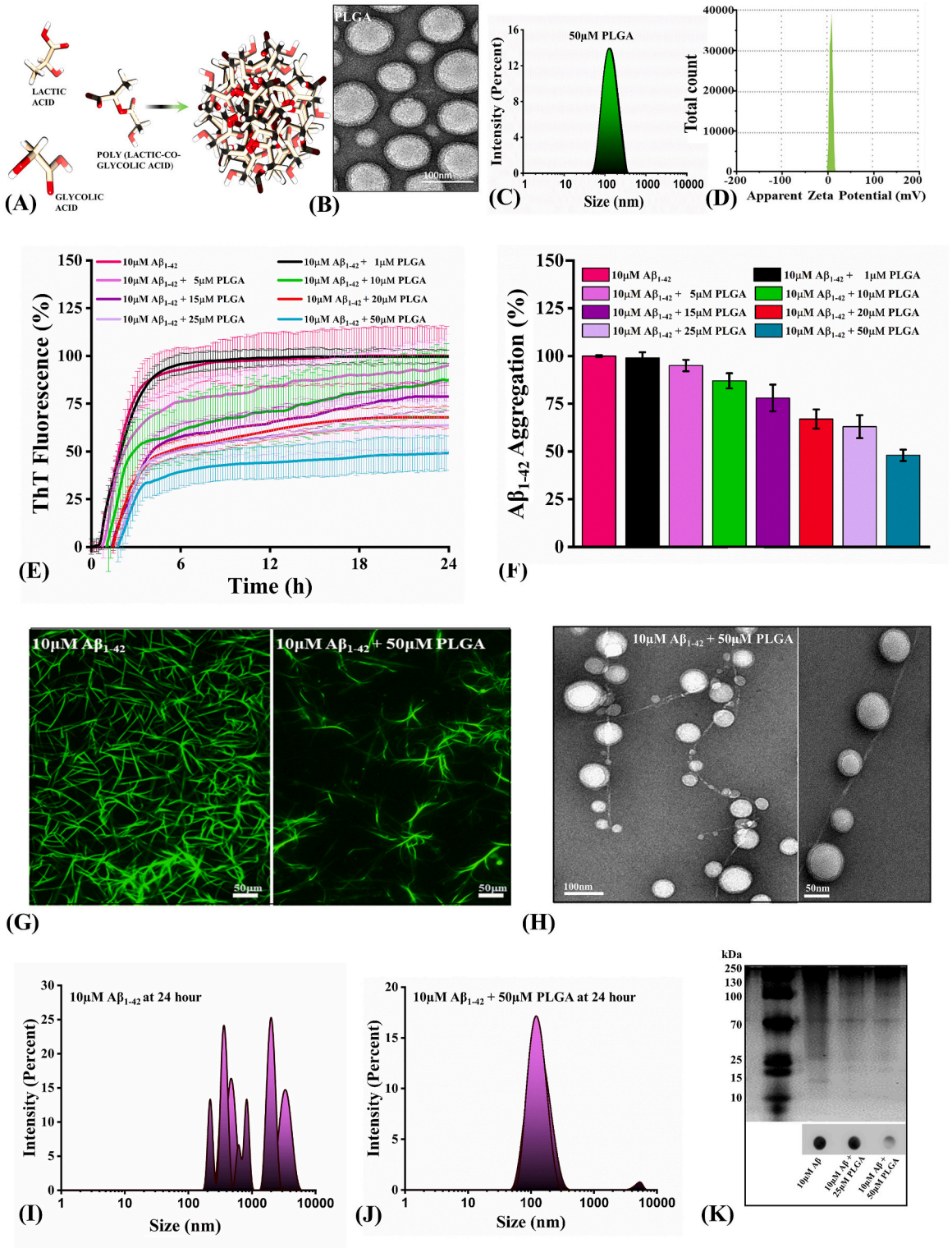

Fig. 2. Attenuation of spontaneous Aβ$_{1-42}$ aggregation by PLGA A; Graphical representation showing the polymerization of poly L-lactic acid and poly L-glycolic acid to form PLGA nanoparticles. **B;** TEM images showing the spheroidal nature of PLGA nanoparticles with an average diameter of ~100 nm. **C:** DLS histogram of the PLGA nanoparticles displaying the diameter size of ~100 nm. **D;** Zeta potential measurement for PLGA nanoparticles revealing the surface charge of ~8 mV. **E & F;** PLGA dose-dependently (1–50 μM) attenuates spontaneous aggregation of 10 μM Aβ$_{1-42}$ as revealed by ThT fluorescence assay over the 24h reaction period. **G;** ThT-stained fluorescence images depicting attenuation of 10 μM Aβ$_{1-42}$ aggregation over 24h in the absence and presence of 50 μM PLGA. **H;** TEM micrograph showing direct association of PLGA nanoparticles with Aβ$_{1-42}$ fibers. **I & J;** DLS analysis revealing hydrodynamic radius of 10 μM Aβ$_{1-42}$ in the absence (I) and presence of 50 μM PLGA (J). Note the decrease in the hydrodynamic radius of Aβ$_{1-42}$ fibers in the presence of PLGA nanoparticles. **K;** Native PAGE showing the loss of higher-ordered Aβ aggregates in the presence of PLGA and the corresponding filter-trap assay (in the inset) revealing decreased formation of Aβ$_{1-42}$ fibers in the presence of PLGA as detected by fibril-specific OC antibody.

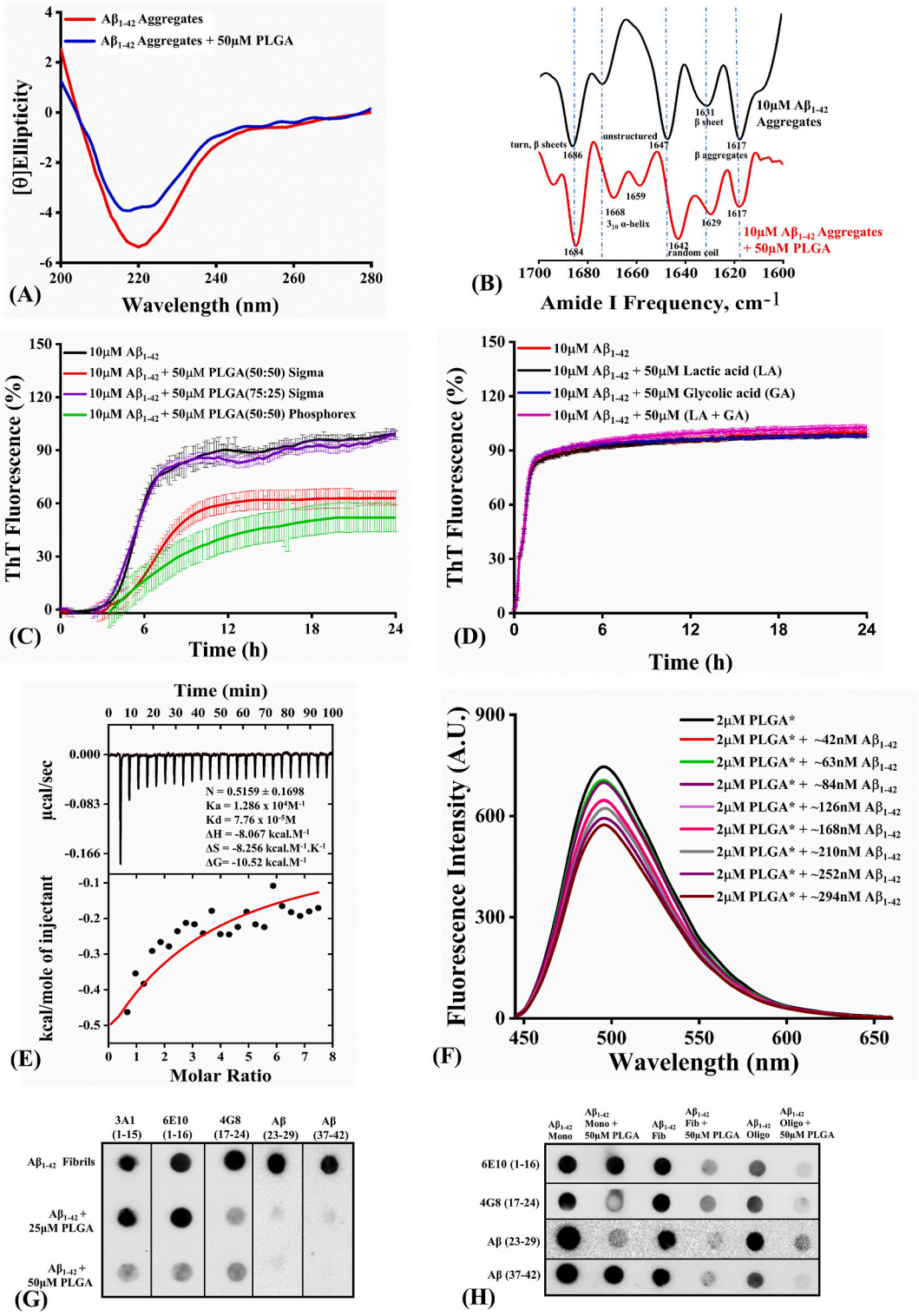

Fig. 3. Characterization of molecular interactions between Aβ$_{1-42}$ and PLGA A; CD spectra showing decreased beta-sheet formation following incubation of 10 μM Aβ$_{1-42}$ in the presence of 50 μM PLGA nanoparticles. **B;** FTIR secondary derivative spectra of the aggregating Aβ$_{1-42}$ samples in the presence (red) and absence (black) of PLGA nanoparticles. Note the dominance of beta-rich signals after aggregation of Aβ$_{1-42}$ and the occurrence of 3_{10} α-helix in the presence of PLGA. **C;** ThT kinetic assays showing that PLGA with 50:50 resomer from Phosphorex (green) and Sigma (red), but not PLGA with 75:25 resomer (purple color), was able to suppress spontaneous aggregation of 10 μM Aβ$_{1-42}$. **D;** ThT kinetic graphs showing that aggregation of 10 μM Aβ$_{1-42}$ was not altered by the presence of 50 μM lactic acid, 50 μM glycolic acid or a mixture of 50 μM lactic acid + glycolic acid. **E;** Isothermal titration calorimetry data obtained after base-line subtraction for the titration of 600 μM PLGA with 10 μM Aβ$_{1-42}$ at 37 °C. The data were plotted for a single-site binding model and the thermodynamic parameters for the protein and ligand complex interaction are presented in the inset. **F;** Decreased fluorescence emission of fluorescent PLGA nanoparticles in the presence of Aβ$_{1-42}$ monomers revealing the quenching effect during the interaction. **G;** Epitope mapping using a filter-trap assay revealing that PLGA nanoparticles interact primarily with the hydrophobic domain of Aβ$_{1-42}$. **H;** Epitope mapping of different Aβ$_{1-42}$ conformers (i.e., monomer, oligomer and fiber) using filter-trap assay revealing that interaction of 50 μM PLGA with Aβ monomer is somewhat more site-specific than Aβ oligomers and aggregates.

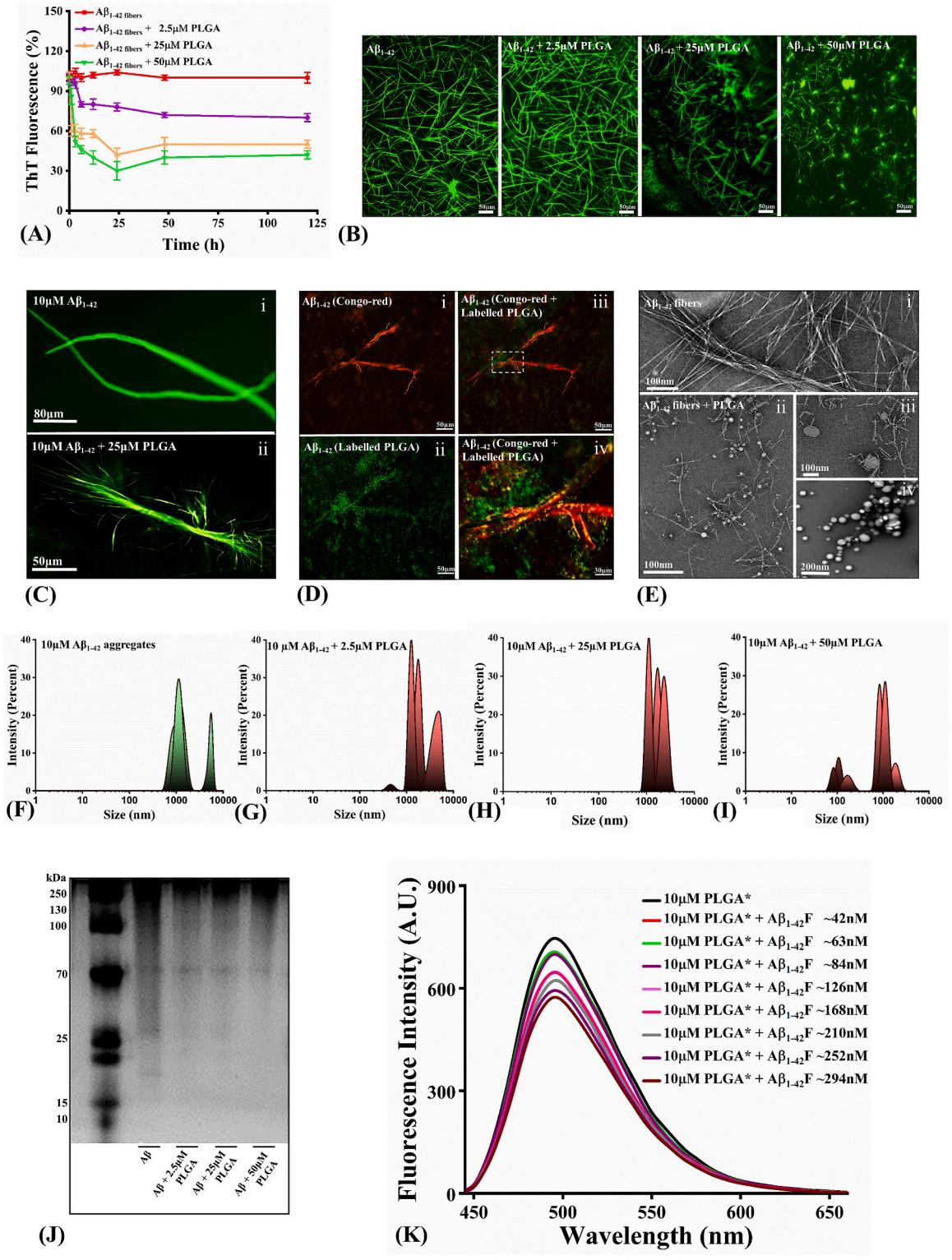

Fig. 4. Disassembly of aggregated Aβ$_{1-42}$ fibers by PLGA A & B; PLGA dose-dependently (2.5–50 μM) triggered disassembly of aggregated Aβ$_{1-42}$ as revealed by the ThT fluorescence assay (A) and ThT-stained fluorescence images (B). **C;** ThT stained images of matured Aβ$_{1-42}$ fibers before (i) and after (ii) treatment with 25 μM PLGA revealing the untwining effect following disassembly. **D;** Fluorescence imaging of Congo red-stained Aβ$_{1-42}$ fibers in the presence of green fluorescent PLGA showing a direct interaction between Aβ$_{1-42}$ fibers and PLGA (i-iv). **E;** TEM images of matured Aβ$_{1-42}$ fibers in the absence (i) and presence of 50 μM PLGA (ii-iv) depicting the direct interaction of the nanoparticles with Aβ fibers. **F–I;** DLS analysis revealing the hydrodynamic radius of 10 μM Aβ$_{1-42}$ aggregates in the absence (F) and presence of 2.5 μM (G), 25 μM (H) and 50 μM (I) PLGA. Note the shift in the hydrodynamic radius of Aβ$_{1-42}$ fibers towards the lower ordered species and possible release of monomers in the presence of PLGA nanoparticles. **J;** Native PAGE analysis of 10 μM Aβ$_{1-42}$ aggregates in the absence and presence of different concentrations (2.5–50 μM) of PLGA. Note the loss of higher-ordered Aβ$_{1-42}$ entities following incubation with PLGA. **K;** Fluorescence quenching effect of labelled PLGA in the presence of increasing concentrations of matured Aβ$_{1-42}$ fibers displaying a decrease in fluorescence intensity, suggesting an interaction between PLGA and Aβ$_{1-42}$ fibers.

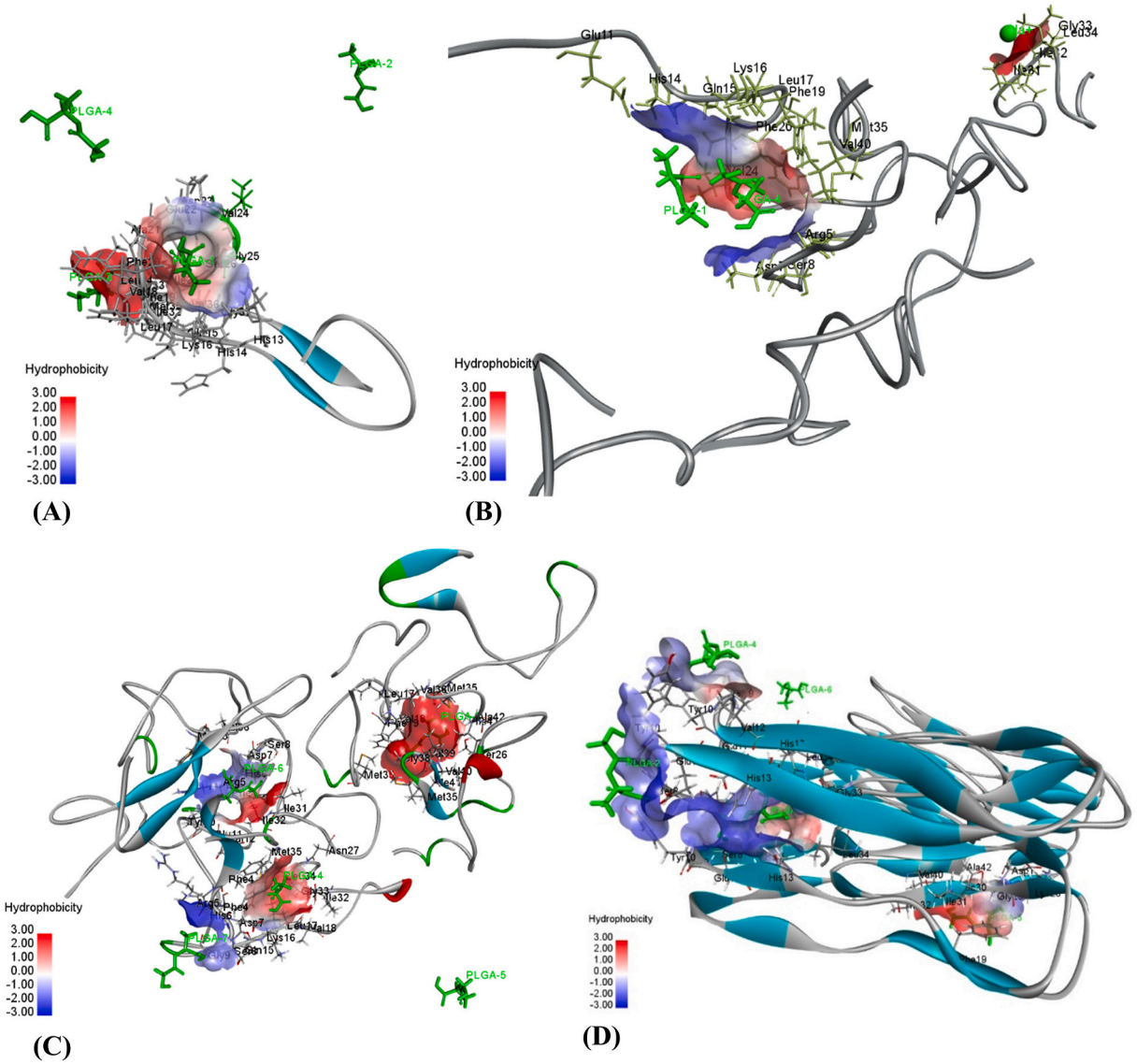

Fig. 5. $A\beta_{1-42}$ binding sites predicted by AutoDock/Chimera and observed after post-docking MD simulations A; Monomer $A\beta_{1-42}$ with two PLGA molecules remaining attached and two detached after 30ns of MD simulations. **B;** Tetramer formed from the solution of eight Aβ peptides and two PLGA molecules attached to it after 30ns long simulations. **C;** Aβ oligomer with four PLGA molecules bound to it. **D;** Fibril fragment with four PLGAs attached and two detached after 70ns of MD simulations. PLGA molecules are highlighted in green and residues of Aβ peptides involved in docking are shown in grey. Colored surfaces depict hydrophobicity of Aβ binding cavities (blue - hydrophilicity, red - hydrophobicity). Aβ peptides are shown in ribbon representation. β-strands are indicated with teal color and random coils and turns in grey.

C-termini, but not the acidic residues E11, E22 and D23, which are involved in all other systems (Sup. Fig. S13; Sup. Table S2).

Structural reorganizations were observed in all systems during post-docking MD simulations (Sup. Fig. S12; Sup. Table S2). In the Aβ monomer only one out of eight original PLGA-Aβ bonds remained, but two new bonds were formed involving residues E11 and E22, which are crucial for oligomerization and fibril formation. In the solution of monomeric Aβ peptides, all PLGA-Aβ bonds predicted from docking were lost; however, some PLGA molecules re-bound at different locations in the course of 30ns MD simulations. The re-binding involved Aβ residues K16-L17 and a hydrophobic pocket of a self-assembled Aβ tetramer. In the Aβ octamer system the PLGA-Aβ bonds predicted by docking were more stable. Four remaining bonds involved Aβ's C-terminal residues and one from the N-terminus. In the fibril system two PLGAs detached, two remained bound to edges of the fibril and two others remained docked inside the fibril, in the gap caused by the removal of one Aβ peptide. The access of PLGA molecules to the interior regions of the fibril might trigger a change of its shape and widening of the gaps. Following post-docking MD simulations, the bonding includes residues Y10-E11 of the Aβ fibril (Fig. 5A–D). Interestingly, dynamic coupling between PLGA molecules and the fibril is substantially non-local and may extend over remote regions of the fibril relative to specific binding sites (Sup. Fig. S13).

3.7. *PLGA-mediated attenuation of Aβ aggregation protects cultured neurons*

Consistent with previous data [10,40,55,56], we showed that 24h treatment of mouse cortical neurons with 1–10 μM $A\beta_{1-42}$ can dose-dependently induce toxicity as evident by a reduction in MTT values and an increase in LDH levels (Fig. 6A and B). Conversely, treatment of cultured neurons with 5–25 μM native PLGA did not reveal any toxic effect following 24h exposure to cultured neurons (Sup. Fig. S14A and B). In parallel, we showed that cultured neurons exposed

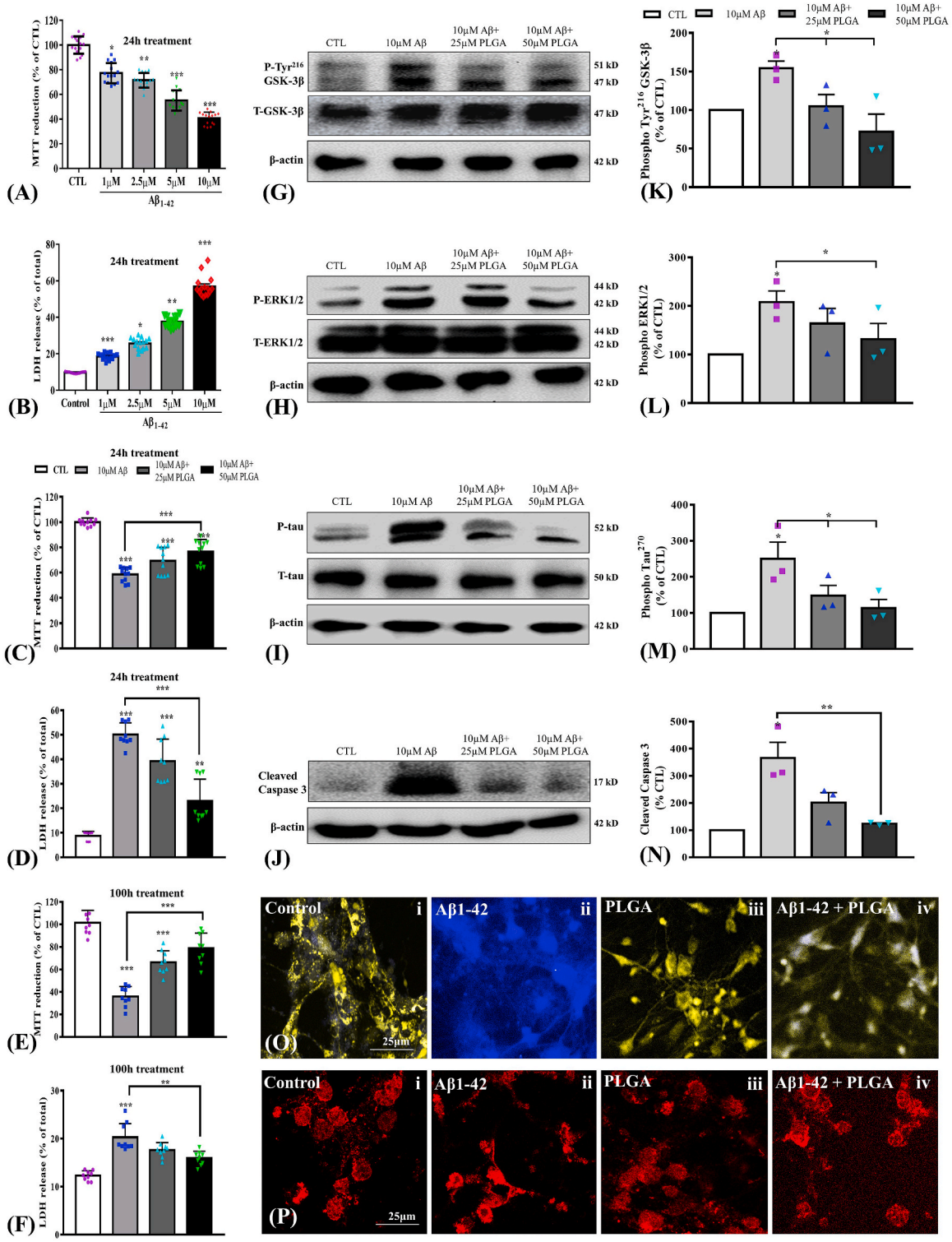

Fig. 6. Attenuation of $A\beta_{1\text{-}42}$ aggregation by PLGA protects cultured neurons A & B; Histogram depicting dose-dependent decrease in the viability of mouse cortical cultured neurons following 24h exposure with oligomeric human $A\beta_{1\text{-}42}$ compared to neurons treated with 10 μM $A\beta_{42\text{-}1}$ (Cont) as revealed by MTT (A) and LDH (B) assays. **C–F;** Histograms showing protection of mouse cortical cultured neurons after 24h (C, D) and 100h (E, F) treatment with 10 μM $A\beta_{1\text{-}42}$ exposed to 25 and 50 μM PLGA as detected with MTT (C, E) and LDH (D, F) assays. **G-N;** Immunoblots and corresponding histograms showing that protective effects following attenuation of spontaneous Aβ aggregation by PLGA are mediated by decreasing Phospho-Tyr GSK-3β (G, K), Phospho-ERK1/2 (H, L), Phospho-tau (I, M) and cleaved-caspase-3 (J, N) levels. **O;** LysoSensor labelling of mouse cortical cultured neurons in the absence of $A\beta_{1\text{-}42}$ (i), after treatment with 10 μM $A\beta_{1\text{-}42}$ following 24h aggregation (ii), after treatment with 25 μM PLGA (iii) and after treatment with 10 μM $A\beta_{1\text{-}42}$ incubated with 25 μM PLGA for 24h (iv). Note that attenuation of Aβ aggregation by PLGA partially reversed the basic pH environment observed in $A\beta_{1\text{-}42}$-treated neurons. **P;** Confocal microscopy showing distribution of immunoreactive cathepsin D in the absence of $A\beta_{1\text{-}42}$ (i), after treatment with 10 μM $A\beta_{1\text{-}42}$ following 24h aggregation (ii), after treatment with 25 μM PLGA (iii) and after treatment with 10 μM $A\beta_{1\text{-}42}$ incubated with 25 μM PLGA for 24h (iv). Note that PLGA partially reversed cytosolic cathepsin D labelling in Aβ-treated neurons. All results, which are presented as means ± SEM, were obtained from three to five separate experiments. $^{*}p < 0.05$, $^{**}p < 0.01$, $^{***}p < 0.001$.

to 10 μM $A\beta_{1-42}$ samples treated with 25 μM or 50 μM PLGA for either 24h or 100h exhibited significant increase in neuronal viability (Fig. 6C–F). The protective effect is mediated by decreased activation of extracellular-signal-related kinase 1⁄2 (ERK1/2), glycogen synthase kinase (GSK-3β), phosphorylation of tau protein and cleavage of caspase-3 – cellular mechanisms underlying Aβ-induced toxicity (Fig. 6G-N) [10,57]. LysoSensor labelling further revealed that PLGA treated $A\beta_{1-42}$ samples markedly restored the lysosomal acidic environment in Aβ-treated cultured neurons (Fig. 6O). Our results further showed that PLGA-treated Aβ samples could decrease the cytosolic distribution of cathepsin D, indicating a partial reversal of lysosomal leakage/breakdown in Aβ-treated cultured neurons (Fig. 6P). In parallel, we showed that the PLGA-induced disassembly of matured Aβ fibers (i.e., after 24h and 120h incubation) could significantly increase neuronal viability compared to aggregated fibers (Sup. Fig. S14C–F).

3.8. PLGA attenuates AD-related pathology in 5xFAD mice

In agreement with earlier studies involving PLGA encapsulated drugs/agents [21,58,59], chronic icv administration of native PLGA did not lead to fluctuations in body weight, abnormal behavior or adverse clinical signs, suggesting that PLGA at the given dose is safe and non-toxic. To examine if PLGA administration can influence Aβ pathology in 5xFAD mice, we measured the cortical Aβ plaque load labelled with OC and 4G8 antibodies in CSF- and PLGA-treated 5xFAD mice (Fig. 7A). Our quantitative analysis revealed that the number, percentage of areas occupied and the average size of Aβ plaques are significantly reduced in PLGA-treated 5xFAD mice (Fig. 7A–D). In parallel, the levels of APP holoprotein and its cleaved products, i.e., C-terminal fragment-α (CTFα) and CTFβ were decreased in cortex, but not in the unaffected cerebellum of PLGA-treated 5xFAD mice (Fig. 7E–I). The levels of APP, CTFα or CTFβ, however, did not differ significantly either in the cortex or in the cerebellum of CSF- and PLGA-treated WT mice (Fig. 7E–I). Interestingly, the steady-state levels of $A\beta_{1-40}$ and $A\beta_{1-42}$ accompanying the plaque load were found to be markedly decreased in the cortex, but not in the cerebellum, of PLGA-treated 5xFAD mice (Fig. 7J and K). Additionally, our results revealed that fluorescently labelled native PLGA following acute intracerebellar injection interacts directly with a subset of extracellular Aβ-containing neuritic plaques immunolabelled with aggregate specific OC antibody in 5xFAD mice, validating our *in vitro* findings on the interaction between PLGA and Aβ peptide. In contrast to 5xFAD mice, fluorescently labelled PLGA did not accumulate in the brain of control mice (Sup. Fig. S14G and H). It is, however, of interest to note that these data do not exclude the interaction of PLGA with other proteins/molecules.

3.9. PLGA attenuates novel object recognition deficits in 5xFAD mice

Memory deficits represent one of the main clinical symptoms of AD [1,2]. As reported in AD patients, 5xFAD mice exhibit object recognition memory deficits starting at 2.5months of age [60]. To determine if PLGA can attenuate memory deficits, we performed a novel-object memory test in WT and 5xFAD mice following 28 days administration of native PLGA. As expected, 5xFAD mice displayed impaired recognition memory, as evident by a decreased discrimination index to a novel object 24h after training with two similar objects. PLGA-administered 5xFAD mice, on the other hand, spent more time on the novel object than on the familiar object, indicating that the impairment of non-spatial working memory in 5xFAD mice can be attenuated by native PLGA. The memory index in WT mice, however, was not affected by PLGA administration. The effect of PLGA on 5xFAD mice was apparent in the absence of any alteration in exploratory activity between groups during the initial exposure period or between trials (Fig. 7L, M).

3.10. PLGA protects iPSC-derived AD cultured neurons

Disease-specific iPSCs have provided new opportunities for not only recapitulating the disease phenotype but also evaluating novel treatment strategies to prevent the development/progression of the disease pathology [41,61]. Thus, we used iPSC-derived neuronal cultures from two healthy controls and two sporadic AD patients to investigate if native PLGA can rescue AD-related features and/or protect AD neurons from toxicity (Fig. 8A-O). The iPSCs were first differentiated into neural progenitor stem cells and then to neurons as evidenced by the expression of pan-axonal neurofilament SMI-312, neuron-specific class III β-tubulin, microtubule-associated protein 2 (MAP2) and neuronal nuclei NeuN markers (Fig. 8A). In keeping with earlier results [41,62], we showed that neurons of sporadic AD exhibited significantly higher cellular levels of $A\beta_{1-40}$ (Fig. 8B) and phospho-tau (Fig. 8J, N) compared to control neurons. The secretory levels of $A\beta_{1-40}$ were also found to be markedly higher in cultured neurons from one sporadic AD patient (i.e., SAD2-3) but not in the other case (i.e, SAD1-3) compared to healthy controls (Fig. 8C). We subsequently showed that 5 μM $A\beta_{1-42}$ following 24h exposure can induce toxicity in both control and AD neurons (Fig. 8D and E). The effect, similar to that in mouse primary neurons, is mediated by the phosphorylation of ERK1⁄2, GSK-3β and tau protein as well as cleavage of caspase-3 (Fig. 8H-O, Sup. Fig. S15A–H). Our results further indicate that 50 μM PLGA-treated Aβ samples following either 24h or 100h exposure markedly increased viability of control and AD neurons (Fig. 8D–G). This is partly mediated, as evident from cultured samples exposed for 24h to $A\beta_{1-42}$ with or without 50 μM PLGA, by attenuating phosphorylation of tau kinases and tau protein as well as cleaved-caspase-3 levels (Fig. 8H-O; Sup. Fig. S15A–H).

4. Discussion

The present study revealed that FDA-approved biodegradable PLGA nanoparticles without conjugation with any drug or agent can ameliorate not only Aβ aggregation/toxicity but also AD-related pathology in cellular and animal models of AD. This is supported by results which show that: i) PLGA inhibits spontaneous Aβ aggregation and triggers the disassembly of mature $A\beta_{1-42}$ fibers, ii) spectroscopic studies, biochemical analyses and MD simulations depict PLGA interacts with the hydrophobic domain of $A\beta_{1-42}$ (i.e., Lys_{16} to Ala_{21}), precluding a conformational shift towards β-sheet structure, iii) PLGA-treated $A\beta_{1-42}$ samples increase neuronal viability by reducing activation of tau kinases and tau phosphorylation, iv) chronic icv administration of PLGA reverses cognitive deficits and attenuates Aβ levels as well as plaque load in 5xFAD mice and v) PLGA protects iPSC-derived neurons of AD patients against Aβ toxicity by decreasing phosphorylation of tau protein and its associated signaling mechanism. Collectively, these results suggest that native PLGA may have unique therapeutic potential in the treatment of AD pathology.

The mechanism by which Aβ peptides interact with another molecule depends on the hydrophobic/hydrophilic character of the molecules [63]. Previous studies have shown that PLGA encapsulated or conjugated drugs/agents can inhibit Aβ aggregation and toxicity, but the effects have been attributed mostly to the interaction of the drugs with Aβ rather than to PLGA [17,19–22,59,64,65]. Our results showed that native PLGA can suppress fibrillization of both normal and mutant human Aβ peptides, leading to the generation of shorter/fragmented fibrils. This could be due to the interaction of PLGA with Aβ monomers, precluding monomer-monomer hydrogen bonding or hydrophobic interactions preventing the development of critical nuclei and the elongation of fibrils. It is also possible that PLGA could destabilize the initial assembly to form a β-sheet rich scaffold during nucleation leading to an equilibrium shift towards the monomeric phase, which may render the elongation process energetically unfavorable. Thus, PLGA allows Aβ peptides to remain in the monomeric state as apparent by alterations in signals for α-helical *vs* β-sheet structures in CD and FTIR analyses. Due to

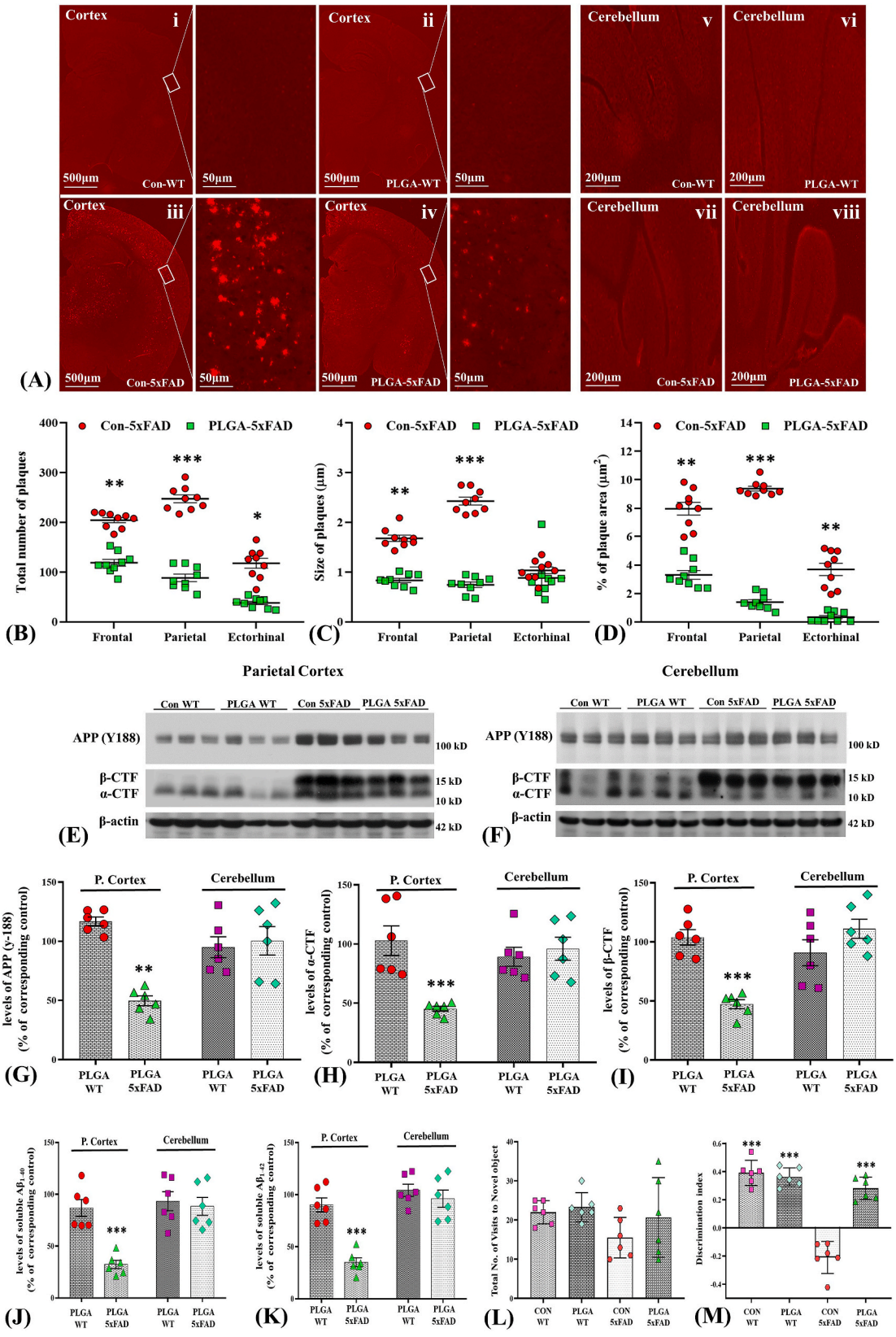

(caption on next page)

Fig. 7. PLGA attenuates AD-related cognitive deficit and pathology in 5xFAD mice A; Photomicrographs depicting OC antibody labelled Aβ deposits in the cortex (i-iv) and cerebellum (v-viii) of PLGA- and CSF-treated WT and 5xFAD mouse brain tissues. As expected, Aβ deposits are evident in the cortex (iii) but not in the cerebellum (vii) of 5xFAD mouse brains. WT mice did not display Aβ deposits in any brain regions (i, v). **B-D;** Histograms showing the quantification of OC antibody labelled Aβ plaques number (B), size (C) and areas occupied (D) in the cortical (i.e., frontal, parietal and entorhinal) regions of PLGA- and CSF-treated 5xFAD mice. Note the decreased number/size and areas occupied by Aβ-containing neuritic plaques in PLGA-treated 5xFAD mice compared to CSF- treated 5xFAD mice. **E-I;** Immunoblots (E, F) and their quantification (G–I) showing the levels of APP holoprotein (Y188) and APP-CTFs (i.e., αCTF and βCTF) in the parietal cortex (E) and cerebellum (F) of PLGA- and CSF-treated 5xFAD mouse brain tissues. Note the decreased levels of APP and its cleaved products in the cortex of PLGA-treated 5xFAD mice compared to CSF-treated 5xFAD mice (G–I). The quantifications of the respective blots were represented as a percentage of the corresponding control group (G–I). **J & K;** Histograms depicting decreased cortical, but not cerebellar, levels of $A\beta_{1\text{-}40}$ (J) and $A\beta_{1\text{-}42}$ (K) in PLGA-treated 5xFAD mice compared to CSF-treated 5xFAD mice. **L & M;** Histograms showing the reversal of object recognition memory following PLGA treatment in 5xFAD mice. The data represent the total number of visits to novel object (L) and the discrimination index (M) from familiar to the novel object of PLGA- and CSF-treated animals. All data expressed as mean ± SEM were obtained from three replicates. CSF, artificial cerebrospinal fluid; WT, wildtype. $^{*}p < 0.05$, $^{**}p < 0.01$, $^{***}p < 0.001$.

the strong hydrophobicity of Aβ, the interaction with the hydrophobic surface of native PLGA could induce Aβ to adopt random coil or native α-helix conformations as a consequence of H-bonding in the nonpolar domain of the peptide that is oriented toward the surface [66] and preclude its ability to form fibrils. The chirality of PLGA possibly induces binding with the Aβ peptide, resulting in the formation of a stable α-helical structure through π-π and hydrophobic interactions. Thus, native PLGA, as observed for some other nanoparticles [67,68], could lead to Aβ absorption and decreased aggregation kinetics. This is supported partly by our MD simulations, where PLGA molecules have been shown to bind easily to various forms of Aβ. Although most of the attachments do not last long, frequent re-binding tends to block the sites that otherwise are actively involved in aggregation. Thus, a conformational switch to a well-organized cross-β structure is precluded by triggering contacts between PLGA and the aggregation-prone aromatic amino acids in the hydrophobic domain of $A\beta_{1\text{-}42,}$ leading to the suppression of Aβ fibril formation.

It is reported that the hydrophobicity of the Aβ increases once it forms oligomers and fibrils [10,69]. Apart from the hydrophobic Lys_{16} to Ala_{21} domain, certain other residues such as His_{14}, Gln_{15}, Ala_{30}, Ile_{31}, Met_{35} and Val_{36} have been shown to play a role in the Aβ oligomerization and fibril formation. The C terminal domain is also involved in the formation of the protofilament structures due to generation of a hydrophobic core between the residues Ile_{41} and Val_{39} with the adjacent fibril. The N terminal domain of a fibril close to the C terminal domain of another fibril may also induce the formation of a salt bridge through intermolecular interactions between Asp_1 and Lys_{28} – an interaction that stabilizes the interface between the two protofilaments [30,70]. Our analysis revealed that PLGA, as observed with a variety of phytochemicals and other molecules [71–75], can interfere with salt bridges and with residues present in the steric zipper domain, an interaction that can trigger disassembly of the preformed fibrillar structure.

Evidence suggests that Aβ aggregates, especially metastable oligomers of different sizes that precede fibril formation, are highly toxic to neurons, whereas monomers or full-length fibrils induce limited toxicity [51,52,76]. We showed that PLGA, by suppressing Aβ aggregation, can protect cultured neurons against toxicity, an effect mediated partly by reducing phosphorylation of tau protein and its associated signaling pathway. In parallel, PLGA treatment partially restores lysosomal integrity/pH is supported by results showing that i) LysoSensor labeling reinstates a more acidic milieu in neurons treated with Aβ aggregates and ii) diminishes the lysosomal egress of immunoreactive cathepsin D observed following Aβ treatment [40]. Disassembly of aggregated Aβ fibers by PLGA also attenuates cell toxicity compared to aggregated fibers alone, thus implicating a therapeutic role for native PLGA in regulating Aβ-mediated toxicity.

Since PLGA suppresses Aβ aggregation and toxicity under *in vitro* conditions, we evaluated the interaction of native PLGA with Aβ aggregates deposited in brains of 5xFAD mice. Our results showed that fluorescent PLGA, following acute administration, accumulates in Aβ-labelled neuritic plaques, suggesting *in vivo* interaction between native PLGA and Aβ peptide as observed under *in vitro* paradigms. Subsequently, we evaluated the ability of native PLGA to attenuate Aβ plaque load as well as impaired cognitive function in 5xFAD mice following 28 days of icv administration. The 5xFAD mice exhibit cognitive deficits along with Aβ deposits starting from the age of 2.5months [40,44,60,77]. Throughout our study, PLGA administration did not cause any abnormal physical signs or behaviors, validating its biocompatibility under *in vivo* conditions [58]. PLGA treatment, however, markedly reduced the area, size and number of Aβ plaques in the affected cortical regions of 5xFAD mice compared to CSF-treated 5xFAD mice, which could be due to inhibition of the spontaneous aggregation and/or disassembly of aggregated Aβ peptides. Since this is accompanied by a decreased level of $A\beta_{1\text{-}40}/A\beta_{1\text{-}42}$ as well as the levels of APP and α-/β-CTFs in the cortex of 5xFAD mice, it is likely that PLGA may also influence the plaque load by decreasing the production/levels of Aβ peptides. In contrast to cortex, PLGA did not significantly alter the levels of APP, α-/β-CTFs or $A\beta_{1\text{-}40}/A\beta_{1\text{-}42}$ either in the cerebellum of 5xFAD mice or in any brain regions of WT control mice, suggesting that the effects may be specific to the affected areas associated with increased levels/deposition of Aβ peptides. Concomitantly, PLGA treatment restored non-spatial object memory deficits in 5xFAD mice, which may be the consequence of reduced Aβ levels/deposition. Although additional studies are needed to determine if PLGA can attenuate other aspects of cognitive function and/or pathology, these results provide compelling evidence for further preclinical investigation to reinforce the potential of native PLGA in the treatment of AD pathology.

Multiple studies have shown that iPSC-derived neurons from AD patients, which provide a unique platform to access novel therapeutic candidates, successfully model familial and sporadic AD including increased levels of Aβ peptide, tau kinases and phospho-tau as well as Rab5-positive early endosomes [41,62]. Supporting that notion, our results showed that iPSC-derived neurons from two sporadic AD patients exhibited increased cellular levels of $A\beta_{1\text{-}40}$ and phospho-tau compared to neurons from control cases. Furthermore, we observed that iPSC-derived human neurons were somewhat more susceptible than mouse neurons to $A\beta_{1\text{-}42}$, although the toxicity in both cases is found to be mediated by increased activation of tau-kinases (i.e., ERK1⁄2 and GSK-3β), phosphorylation of tau protein and cleavage of caspase-3. Interestingly, PLGA-treated Aβ samples significantly protect both control and AD neurons against toxicity by reducing tau-associated signaling mechanisms. As the present result is based exclusively on neurons, discounting their interactions with glial or vascular cells, it would be of interest to determine the effects of PLGA in mixed cultures of multiple cell types, mimicking the complexity of the brain. Nevertheless, these results provide unique evidence for the possible application of native PLGA in the treatment of AD pathology.

At present, there is no effective treatment available for AD patients. The cholinesterase inhibitors and the NMDA receptor antagonist memantine that have been approved for treatment provide symptomatic relief only for a subset of AD patients [78,79]. The beneficial effects of recently approved disease-modifying Aβ monoclonal antibody Aducanumab on AD patients remain to be established [80,81]. However, failures of multiple clinical trials over the years targeting Aβ either by vaccination or reduction of its production using inhibitors of β-/γ-secretases have fueled some skepticism [82]. Unlike systemic

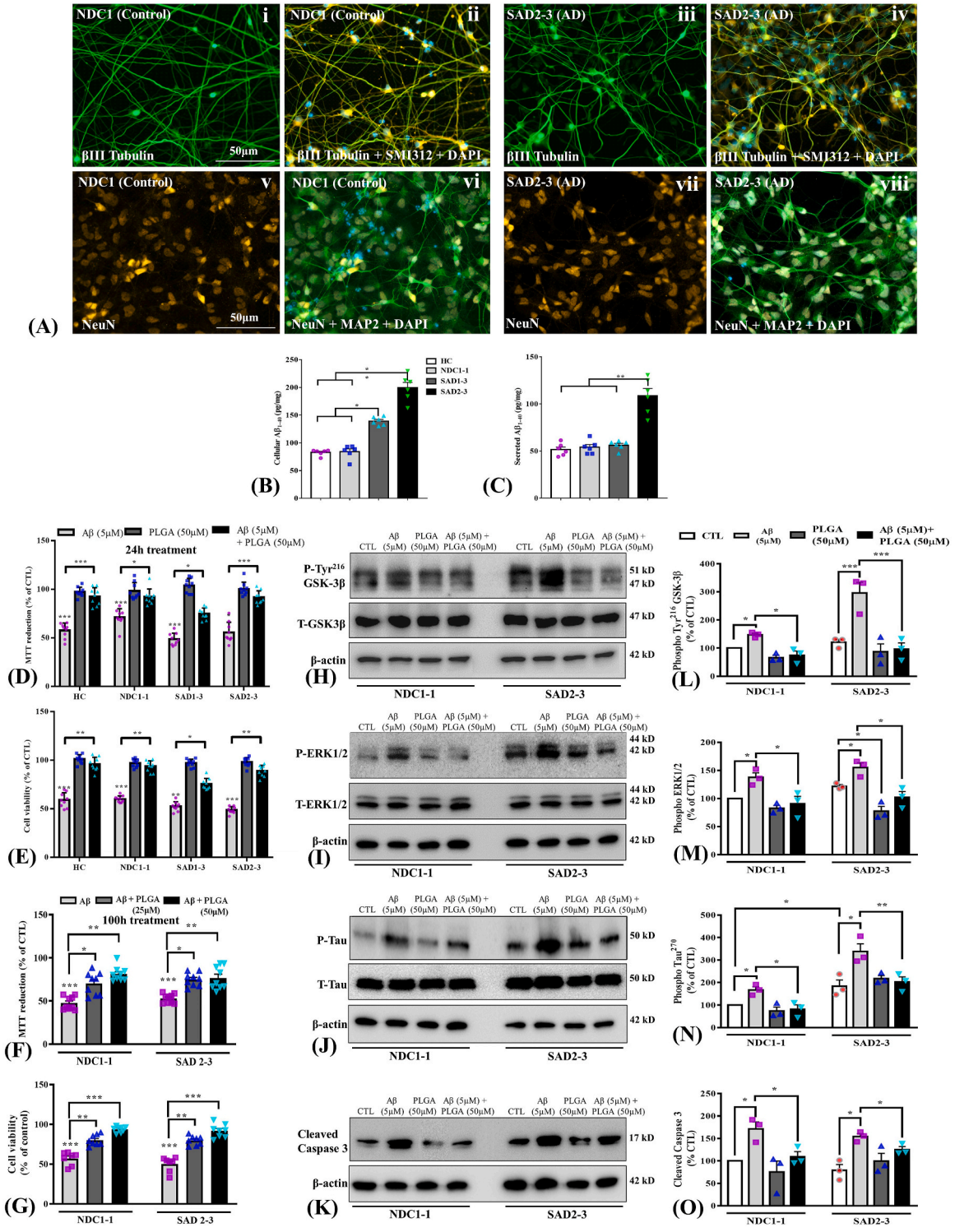

Fig. 8. PLGA protects iPSC-derived AD neurons against Aβ-induced toxicity A; Representative immunofluorescence images of iPSC-derived neurons from a healthy control (i, ii, v, vi) and a sporadic AD patient (iii, iv, vii, viii) labelled with different neuronal markers. The upper panel shows immunofluorescence labelling with βIII Tubulin (neuronal microtubule marker) (i and iii), βIII Tubulin + SMI312 (pan axonal marker) + DAPI (nuclear marker) (ii and iv), whereas the lower panel reveals immunofluorescence labelling with NeuN (neuronal nuclear marker)(v and vii), NeuN + MAP2 (dendritic marker) + DAPI (vi and viii) in iPSC-derived control and sporadic AD neurons. **B & C;** Histograms showing the cellular (B) and secretory (C) levels of human $A\beta_{1\text{-}40}$ in iPSC-derived primary neurons from two control and two sporadic AD-patients. Note the significant increase in cellular $A\beta_{1\text{-}40}$ levels in both iPSC-AD neurons, while the secretory $A\beta_{1\text{-}40}$ level was found to be increased only in one case of iPSC-AD neurons compared to controls. **D & E;** Histograms showing protection of cultured neurons derived from control and sporadic AD following 24h exposure to 5 μM $A\beta_{1\text{-}42}$ with or without 25 and 50 μM PLGA as detected with MTT (D) and cell toxicity (E) assays. **F & G;** Histograms showing protection of cultured neurons derived from control and sporadic AD following 100h exposure to 5 μM $A\beta_{1\text{-}42}$ in the presence or absence of 25 and 50 μM PLGA as detected with MTT (F) and cell toxicity (G) assays. **H–O;** Immunoblots and corresponding histograms depicting that protective effect of PLGA in one control and sporadic AD neurons against 5 μM $A\beta_{1\text{-}42}$ following 24h exposure is mediated by decreasing the levels of Phospho-Tyr GSK-3β (H, L), Phospho-ERK1/2 (I, M), Phospho-tau (J, N) and cleaved-caspase-3 (K, O). All data expressed as mean ± SEM were obtained from three-four replicates. $^*p < 0.05$, $^{**}p < 0.01$, $^{***}p < 0.001$.

diseases, a limiting factor for neurodegenerative diseases such as AD is the blood-brain barrier preventing the penetration of potential drugs into the brain [11,16,83]. Considering that Aβ peptides are produced constitutively and have physiological functions in the brain [1,2], it is likely that pursuing Aβ at different stages of pathological progression (i.e., aggregation, disaggregation and neurotoxicity) rather than regulating its production/clearance mechanism or neutralizing a subset of Aβ using epitope-specific antibodies may be more beneficial in the treatment of AD pathology. Recent studies have shown that PLGA nanoparticles conjugated or encapsulated with various drugs/agents such as donepezil, galantamine, quercetin, memantine and curcumin can exhibit positive effects on cellular and/or animal models of AD compared to cells/mice treated with drugs alone or vehicles used for dissolving drugs/PLGA nanoparticles [17–19,21,22,59,65]. However, no study has so far evaluated the effects of native PLGA in cellular and/or animal models of AD despite its satisfactory biocompatibility [20,64]. Intriguingly, the present study reveals that PLGA without conjugation with any agent not only suppresses Aβ aggregation/toxicity and attenuates AD-related pathology in an animal model of AD but also protects human AD neurons against toxicity. Although the effects of PLGA on neurofibrillary tangles remain elusive, reduction of tau-phosphorylation in Aβ-treated cultured neurons as observed in the present study and attenuation of tau aggregation *in vitro* (unpublished data) may suggest a role for PLGA on tau pathology in AD brains. These results, taken together, not only highlight the significance of native PLGA in targeting different facets of Aβ pathology, but also suggest its unique potential in the treatment of AD, which overwhelms our aging population.

5. Conclusion

The present study using multiple approaches showed that FDA-approved biodegradable PLGA nanoparticles, used mostly as a drug delivery vehicle, without conjugation with any agent can ameliorate Aβ aggregation/toxicity as well as AD-related pathology in cellular and animal models of AD. These results provide unequivocal evidence that native PLGA, by targeting different aspects of the Aβ axis, can have unique therapeutic potential in the treatment of AD pathology.

Intellectual property

A provisional patent application has been filed in 2020 with help from the University of Alberta for the potential use of PLGA in the treatment of neurodegenerative diseases.

Data availability

The data in this work are available in the manuscript or Supplementary Information, or available from the corresponding author upon reasonable request.

CRediT authorship contribution statement

Bibin Anand: did the experiments and analyzed the data included in the manuscript. **Qi Wu:** did the experiments and analyzed the data included in the manuscript. **Maryam Nakhaei-Nejad:** did the experiments and analyzed the data included in the manuscript. **Govindarajan Karthivashan:** did the experiments and analyzed the data included in the manuscript. **Lyudmyla Dorosh:** did the experiments and analyzed the data included in the manuscript. **Sara Amidian:** did the experiments and analyzed the data included in the manuscript. **Abhishek Dahal:** did the experiments and analyzed the data included in the manuscript. **Xiuju Li:** did the experiments and analyzed the data included in the manuscript. **Maria Stepanova:** as a supervisor, designed the study, helped in analyzing the data and writing the manuscript. **Holger Wille:** as a supervisor, designed the study, helped in analyzing the data and writing the manuscript. **Fabrizio Giuliani:** as a supervisor, designed the study, helped in analyzing the data and writing the manuscript. **Satyabrata Kar:** as a supervisor, designed the study, helped in analyzing the data and wrote the manuscript with help/input from all co-authors involved in the study. , The.

Declaration of competing interest

The authors declare no competing financial interests or personal relationships that could influence the work reported in this paper.

Acknowledgments

This work was supported by a grant from CIHR (MOP-84480) to SK, HW and FG, grants from APRI-ASANT to SK and HW, as well as a SynAD grant to SK and FG. BGA, QW, KG are recipients of SynAD postdoctoral fellowships from the University of Alberta. We would like to extend our gratitude to Drs. G. Baker and S. Ahmad for their constructive criticisms of our manuscript. None of the authors included in this manuscript has had any actual or potential conflict of interest including financial, personal or other relationships with other people or organizations at any time that could inappropriately influence the work.

Appendix A. Supplementary data

Supplementary data to this article can be found online at https://doi.org/10.1016/j.bioactmat.2022.05.030.

References

[1] D.J. Selkoe, J. Hardy, The amyloid hypothesis of Alzheimer's disease at 25 years, EMBO Mol. Med. 8 (6) (2016) 595–608.
[2] C.A. Lane, J. Hardy, J.M. Schott, Alzheimer's disease, Eur. J. Neurol. 25 (1) (2018) 59–70.
[3] C.M. Karch, A.M. Goate, Alzheimer's disease risk genes and mechanisms of disease pathogenesis, Biol. Psychiatr. 77 (1) (2015) 43–51.
[4] J.H. Kim, Genetics of Alzheimer's disease, Dement Neurocogn Disord 17 (4) (2018) 131–136.
[5] D.P. Perl, Neuropathology of Alzheimer's disease, Mt. Sinai J. Med. 77 (1) (2010) 32–42.
[6] J.E. Straub, D. Thirumalai, Toward a molecular theory of early and late events in monomer to amyloid fibril formation, Annu. Rev. Phys. Chem. 62 (2011) 437–463.
[7] F. Bisceglia, A. Natalello, M.M. Serafini, R. Colombo, L. Verga, C. Lanni, E. De Lorenzi, An integrated strategy to correlate aggregation state, structure and toxicity of Ass 1-42 oligomers, Talanta 188 (2018) 17–26.
[8] T.J. Revett, G.B. Baker, J. Jhamandas, S. Kar, Glutamate system, amyloid ss peptides and tau protein: functional interrelationships and relevance to Alzheimer disease pathology, J. Psychiatry Neurosci. 38 (1) (2013) 6–23.
[9] G.F. Chen, T.H. Xu, Y. Yan, Y.R. Zhou, Y. Jiang, K. Melcher, H.E. Xu, Amyloid beta: structure, biology and structure-based therapeutic development, Acta Pharmacol. Sin. 38 (9) (2017) 1205–1235.
[10] S.J. Lee, E. Nam, H.J. Lee, M.G. Savelieff, M.H. Lim, Towards an understanding of amyloid-beta oligomers: characterization, toxicity mechanisms, and inhibitors, Chem. Soc. Rev. 46 (2) (2017) 310–323.
[11] F. Re, M. Gregori, M. Masserini, Nanotechnology for neurodegenerative disorders, Nanomedicine 8 (1) (2012) S51–S58.
[12] J. Saraf, K. Kalia, P. Bhattacharya, R.K. Tekade, Growing synergy of nanodiamonds in neurodegenerative interventions, Drug Discov. Today 24 (2) (2019) 584–594.
[13] G. Tosi, F. Pederzoli, D. Belletti, M.A. Vandelli, F. Forni, J.T. Duskey, B. Ruozi, Nanomedicine in Alzheimer's disease: amyloid beta targeting strategy, Prog. Brain Res. 245 (2019) 57–88.
[14] F. Danhier, E. Ansorena, J.M. Silva, R. Coco, A. Le Breton, V. Preat, PLGA-based nanoparticles: an overview of biomedical applications, J. Contr. Release 161 (2) (2012) 505–522.
[15] Y. Wang, W. Qu, S.H. Choi, FDA's regulatory science program for generic PLA/PLGA-based drug program, Am. Pharmaceut. Rev. 20 (2016) 4.
[16] D. Ding, Q. Zhu, Recent advances of PLGA micro/nanoparticles for the delivery of biomacromolecular therapeutics, Mater. Sci. Eng. C Mater. Biol. Appl. 92 (2018) 1041–1060.
[17] I. Baysal, G. Ucar, M. Gultekinoglu, K. Ulubayram, S. Yabanoglu-Ciftci, Donepezil loaded PLGA-b-PEG nanoparticles: their ability to induce destabilization of amyloid fibrils and to cross blood brain barrier in vitro, J. Neural. Transm. 124 (1) (2017) 33–45.
[18] C. Fornaguera, N. Feiner-Gracia, G. Caldero, M.J. Garcia-Celma, C. Solans, Galantamine-loaded PLGA nanoparticles, from nano-emulsion templating, as novel advanced drug delivery systems to treat neurodegenerative diseases, Nanoscale 7 (28) (2015) 12076–12084.

[19] D. Sun, N. Li, W. Zhang, Z. Zhao, Z. Mou, D. Huang, J. Liu, W. Wang, Design of PLGA-functionalized quercetin nanoparticles for potential use in Alzheimer's disease, Colloids Surf. B Biointerfaces 148 (2016) 116–129.
[20] M.J. Hajipour, M.R. Santoso, F. Rezaee, H. Aghaverdi, M. Mahmoudi, G. Perry, Advances in Alzheimer's diagnosis and therapy: the implications of nanotechnology, Trends Biotechnol. 35 (10) (2017) 937–953.
[21] E. Sanchez-Lopez, M. Ettcheto, M.A. Egea, M. Espina, A. Cano, A.C. Calpena, A. Camins, N. Carmona, A.M. Silva, E.B. Souto, M.L. Garcia, Memantine loaded PLGA PEGylated nanoparticles for Alzheimer's disease: in vitro and in vivo characterization, J. Nanobiotechnol. 16 (1) (2018) 32.
[22] S.G. Jeon, M.Y. Cha, J.I. Kim, T.W. Hwang, K.A. Kim, T.H. Kim, K.C. Song, J.J. Kim, M. Moon, Vitamin D-binding protein-loaded PLGA nanoparticles suppress Alzheimer's disease-related pathology in 5XFAD mice, Nanomedicine 17 (2019) 297–307.
[23] B.V. Foroutanpay, J. Kumar, S.G. Kang, N. Danaei, D. Westaway, V.L. Sim, S. Kar, The effects of N-terminal mutations on beta-amyloid peptide aggregation and toxicity, Neuroscience 379 (2018) 177–188.
[24] R. Wetzel, S. Chemuru, P. Misra, R. Kodali, S. Mukherjee, K. Kar, An aggregate weight-normalized Thioflavin-T measurement scale for characterizing polymorphic amyloids and assembly intermediates, Methods Mol. Biol. 1777 (2018) 121–144.
[25] B.G. Anand, K.P. Prajapati, K. Dubey, N. Ahamad, D.S. Shekhawat, P.C. Rath, G. K. Joseph, K. Kar, Self-assembly of artificial sweetener Aspartame yields amyloid-like cytotoxic nanostructures, ACS Nano 13 (5) (2019) 6033–6049.
[26] B.G. Anand, Q. Wu, G. Karthivashan, K.P. Shejale, S. Amidian, H. Wille, S. Kar, Mimosine functionalized gold nanoparticles (Mimo-AuNPs) suppress β-amyloid aggregation and neuronal toxicity, Bioact. Mater. 6 (12) (2021) 4491–4505.
[27] X. Li, X. Zhang, A.R. Ladiwala, D. Du, J.K. Yadav, P.M. Tessier, P.E. Wright, J. W. Kelly, J.N. Buxbaum, Mechanisms of transthyretin inhibition of beta-amyloid aggregation in vitro, J. Neurosci. 33 (50) (2013) 19423–19433.
[28] J.R. Lakowicz, G. Weber, Quenching of fluorescence by oxygen. A probe for structural fluctuations in macromolecules, Biochemistry 12 (21) (1973) 4161–4170.
[29] S. Kim, J. Chen, T. Cheng, A. Gindulyte, J. He, S. He, Q. Li, B.A. Shoemaker, P. A. Thiessen, B. Yu, L. Zaslavsky, J. Zhang, E.E. Bolton, PubChem 2019 update: improved access to chemical data, Nucleic Acids Res. 47 (D1) (2019) D1102–D1109.
[30] L. Gremer, D. Scholzel, C. Schenk, E. Reinartz, J. Labahn, R.B.G. Ravelli, M. Tusche, C. Lopez-Iglesias, W. Hoyer, H. Heise, D. Willbold, G.F. Schroder, Fibril structure of amyloid-beta(1-42) by cryo-electron microscopy, Science 358 (6359) (2017) 116–119.
[31] C.R. Sondergaard, M.H. Olsson, M. Rostkowski, J.H. Jensen, Improved treatment of ligands and coupling effects in empirical calculation and rationalization of pKa values, J. Chem. Theor. Comput. 7 (7) (2011) 2284–2295.
[32] M. Abraham, D.V.D. Spoel, E. Lindahl, B. Hess, t.G.d. team, GROMACS User Manual Version 2018, 2019.
[33] E.F. Pettersen, T.D. Goddard, C.C. Huang, G.S. Couch, D.M. Greenblatt, E.C. Meng, T.E. Ferrin, UCSF Chimera–a visualization system for exploratory research and analysis, J. Comput. Chem. 25 (13) (2004) 1605–1612.
[34] O. Trott, A.J. Olson, AutoDock Vina, Improving the speed and accuracy of docking with a new scoring function, efficient optimization, and multithreading, J. Comput. Chem. 31 (2) (2010) 455–461.
[35] N. Wilkosz, G. Lazarski, L. Kovacik, P. Gargas, M. Nowakowska, D. Jamroz, M. Kepczynski, Molecular insight into drug-loading capacity of PEG-PLGA nanoparticles for itraconazole, J. Phys. Chem. B 122 (28) (2018) 7080–7090.
[36] W.L. Jorgensen, D.S. Maxwell, J. Tirado-Rives, Development and testing of the OPLS all-Atom force field on conformational energetics and properties of organic liquids, J. Am. Chem. Soc. 118 (45) (1996) 11225–11236.
[37] H.J.C. Berendsen, J.R. Grigera, T.P. Straatsma, The missing term in effective pair potentials, J. Phys. Chem. 91 (24) (1987) 6269–6271.
[38] L. Dorosh, M. Stepanova, Probing oligomerization of amyloid beta peptide in silico, Mol. Biosyst. 13 (1) (2016) 165–182.
[39] A. Amritraj, Y. Wang, T.J. Revett, D. Vergote, D. Westaway, S. Kar, Role of cathepsin D in U18666A-induced neuronal cell death: potential implication in Niemann-Pick type C disease pathogenesis, J. Biol. Chem. 288 (5) (2013) 3136–3152.
[40] Y. Wang, Q. Wu, B.G. Anand, G. Karthivashan, G. Phukan, J. Yang, G. Thinakaran, D. Westaway, S. Kar, Significance of Cytosolic Cathepsin D in Alzheimer's Disease Pathology: Protective Cellular Effects of PLGA Nanoparticles against Beta-Amyloid-Toxicity, Neuropathol Appl Neurobiol, 2020.
[41] M.A. Israel, S.H. Yuan, C. Bardy, S.M. Reyna, Y. Mu, C. Herrera, M.P. Hefferan, S. Van Gorp, K.L. Nazor, F.S. Boscolo, C.T. Carson, L.C. Laurent, M. Marsala, F. H. Gage, A.M. Remes, E.H. Koo, L.S. Goldstein, Probing sporadic and familial Alzheimer's disease using induced pluripotent stem cells, Nature 482 (7384) (2012) 216–220.
[42] S.H. Yuan, J. Martin, J. Elia, J. Flippin, R.I. Paramban, M.P. Hefferan, J.G. Vidal, Y. Mu, R.L. Killian, M.A. Israel, N. Emre, S. Marsala, M. Marsala, F.H. Gage, L. S. Goldstein, C.T. Carson, Cell-surface marker signatures for the isolation of neural stem cells, glia and neurons derived from human pluripotent stem cells, PLoS One 6 (3) (2011), e17540.
[43] Q. Wu, L. Qiao, J. Yang, Y. Zhou, Q. Liu, Stronger activation of SREBP-1a by nucleus-localized HBx, Biochem. Biophys. Res. Commun. 460 (3) (2015) 561–565.
[44] H. Oakley, S.L. Cole, S. Logan, E. Maus, P. Shao, J. Craft, A. Guillozet-Bongaarts, M. Ohno, J. Disterhoft, L. Van Eldik, R. Berry, R. Vassar, Intraneuronal beta-amyloid aggregates, neurodegeneration, and neuron loss in transgenic mice with five familial Alzheimer's disease mutations: potential factors in amyloid plaque formation, J. Neurosci. 26 (40) (2006) 10129–10140.
[45] A. Di Pardo, V. Maglione, M. Alpaugh, M. Horkey, R.S. Atwal, J. Sassone, A. Ciammola, J.S. Steffan, K. Fouad, R. Truant, S. Sipione, Ganglioside GM1 induces phosphorylation of mutant huntingtin and restores normal motor behavior in Huntington disease mice, Proc. Natl. Acad. Sci. U. S. A. 109 (9) (2012) 3528–3533.
[46] C. Hawkes, D. Kabogo, A. Amritraj, S. Kar, Up-regulation of cation-independent mannose 6-phosphate receptor and endosomal-lysosomal markers in surviving neurons after 192-IgG-saporin administrations into the adult rat brain, Am. J. Pathol. 169 (4) (2006) 1140–1154.
[47] Q. Wu, Z. Li, P. Mellor, Y. Zhou, D.H. Anderson, Q. Liu, The role of PTEN - HCV core interaction in hepatitis C virus replication, Sci. Rep. 7 (1) (2017) 3695.
[48] A. Kodam, D. Ourdev, M. Maulik, J. Hariharakrishnan, M. Banerjee, Y. Wang, S. Kar, A role for astrocyte-derived amyloid beta peptides in the degeneration of neurons in an animal model of temporal lobe epilepsy, Brain Pathol. 29 (1) (2019) 28–44.
[49] L. Costa-Marques, K. Arnold, M.C. Pardon, C. Leovsky, S. Swarbrick, C. Fabian, A. Stolzing, Transplantation of bone marrow derived macrophages reduces markers of neuropathology in an APP/PS1 mouse model, Transl. Neurodegener. 8 (2019) 33.
[50] M. Maulik, B. Ghoshal, J. Kim, Y. Wang, J. Yang, D. Westaway, S. Kar, Mutant human APP exacerbates pathology in a mouse model of NPC and its reversal by a beta-cyclodextrin, Hum. Mol. Genet. 21 (22) (2012) 4857–4875.
[51] O.V. Galzitskaya, E.I. Galushko, O.M. Selivanova, Studies of the process of amyloid formation by Abeta peptide, Biochemistry (Mosc.) 83 (1) (2018) S62–S80.
[52] P. Arosio, T.P. Knowles, S. Linse, On the lag phase in amyloid fibril formation, Phys. Chem. Chem. Phys. 17 (12) (2015) 7606–7618.
[53] M. Biancalana, S. Koide, Molecular mechanism of Thioflavin-T binding to amyloid fibrils, Biochim. Biophys. Acta 1804 (7) (2010) 1405–1412.
[54] W.E. Van Nostrand, J.P. Melchor, H.S. Cho, S.M. Greenberg, G.W. Rebeck, Pathogenic effects of D23N Iowa mutant amyloid beta -protein, J. Biol. Chem. 276 (35) (2001) 32860–32866.
[55] Z. Wei, M.S. Song, D. MacTavish, J.H. Jhamandas, S. Kar, Role of calpain and caspase in beta-amyloid-induced cell death in rat primary septal cultured neurons, Neuropharmacology 54 (4) (2008) 721–733.
[56] R. Kayed, C.A. Lasagna-Reeves, Molecular mechanisms of amyloid oligomers toxicity, J. Alzheimers Dis. 33 (1) (2013) S67–S78.
[57] M.S. Song, G. Rauw, G.B. Baker, S. Kar, Memantine protects rat cortical cultured neurons against beta-amyloid-induced toxicity by attenuating tau phosphorylation, Eur. J. Neurosci. 28 (10) (2008) 1989–2002.
[58] N. Huang, S. Lu, X.G. Liu, J. Zhu, Y.J. Wang, R.T. Liu, PLGA nanoparticles modified with a BBB-penetrating peptide co-delivering Abeta generation inhibitor and curcumin attenuate memory deficits and neuropathology in Alzheimer's disease mice, Oncotarget 8 (46) (2017) 81001–81013.
[59] S. Fan, Y. Zheng, X. Liu, W. Fang, X. Chen, W. Liao, X. Jing, M. Lei, E. Tao, Q. Ma, X. Zhang, R. Guo, J. Liu, Curcumin-loaded PLGA-PEG nanoparticles conjugated with B6 peptide for potential use in Alzheimer's disease, Drug Deliv. 25 (1) (2018) 1091–1102.
[60] F. Kosel, P. Torres Munoz, J.R. Yang, A.A. Wong, T.B. Franklin, Age-related changes in social behaviours in the 5xFAD mouse model of Alzheimer's disease, Behav. Brain Res. 362 (2019) 160–172.
[61] J. Penney, W.T. Ralvenius, L.H. Tsai, Modeling Alzheimer's disease with iPSC-derived brain cells, Mol. Psychiatr. 25 (1) (2020) 148–167.
[62] A. Ochalek, B. Mihalik, H.X. Avci, A. Chandrasekaran, A. Teglasi, I. Bock, M. L. Giudice, Z. Tancos, K. Molnar, L. Laszlo, J.E. Nielsen, B. Holst, K. Freude, P. Hyttel, J. Kobolak, A. Dinnyes, Neurons derived from sporadic Alzheimer's disease iPSCs reveal elevated TAU hyperphosphorylation, increased amyloid levels, and GSK3B activation, Alzheimer's Res. Ther. 9 (1) (2017) 90.
[63] C.E. Giacomelli, W. Norde, Conformational changes of the amyloid beta-peptide (1-40) adsorbed on solid surfaces, Macromol. Biosci. 5 (5) (2005) 401–407.
[64] S.A. Ansari, R. Satar, A. Perveen, G.M. Ashraf, Current opinion in Alzheimer's disease therapy by nanotechnology-based approaches, Curr. Opin. Psychiatr. 30 (2) (2017) 128–135.
[65] M. Silva-Abreu, A.C. Calpena, P. Andres-Benito, E. Aso, I.A. Romero, D. Roig-Carles, R. Gromnicova, M. Espina, I. Ferrer, M.L. Garcia, D. Male, PPARgamma agonist-loaded PLGA-PEG nanocarriers as a potential treatment for Alzheimer's disease: in vitro and in vivo studies, Int. J. Nanomed. 13 (2018) 5577–5590.
[66] L.C. Serpell, Alzheimer's amyloid fibrils: structure and assembly, Biochim. Biophys. Acta 1502 (1) (2000) 16–30.
[67] C. Cabaleiro-Lago, F. Quinlan-Pluck, I. Lynch, S. Lindman, A.M. Minogue, E. Thulin, D.M. Walsh, K.A. Dawson, S. Linse, Inhibition of amyloid beta protein fibrillation by polymeric nanoparticles, J. Am. Chem. Soc. 130 (46) (2008) 15437–15443.
[68] Y.H. Liao, Y.J. Chang, Y. Yoshiike, Y.C. Chang, Y.R. Chen, Negatively charged gold nanoparticles inhibit Alzheimer's amyloid-beta fibrillization, induce fibril dissociation, and mitigate neurotoxicity, Small 8 (23) (2012) 3631–3639.
[69] J. Lee, E.K. Culyba, E.T. Powers, J.W. Kelly, Amyloid-beta forms fibrils by nucleated conformational conversion of oligomers, Nat. Chem. Biol. 7 (9) (2011) 602–609.
[70] E.Y. Hayden, K.K. Hoi, J. Lopez, M. Inayathullah, M.M. Condron, D.B. Teplow, Identification of key regions and residues controlling Abeta folding and assembly, Sci. Rep. 7 (1) (2017), 12434.
[71] A. Thapa, S.D. Jett, E.Y. Chi, Curcumin attenuates amyloid-beta aggregate toxicity and modulates amyloid-beta aggregation pathway, ACS Chem. Neurosci. 7 (1) (2016) 56–68.
[72] S. Andarzi Gargari, A. Barzegar, A. Tarinejad, The role of phenolic OH groups of flavonoid compounds with H-bond formation ability to suppress amyloid mature

fibrils by destabilizing beta-sheet conformation of monomeric Abeta17-42, PLoS One 13 (6) (2018), e0199541.
[73] S. Andrade, M.J. Ramalho, J.A. Loureiro, M.D.C. Pereira, Natural compounds for Alzheimer's disease therapy: a systematic review of preclinical and clinical studies, Int. J. Mol. Sci. 20 (9) (2019) 2313.
[74] P.K. Kanchi, A.K. Dasmahapatra, Polyproline chains destabilize the Alzheimer's amyloid-beta protofibrils: a molecular dynamics simulation study, J. Mol. Graph. Model. 93 (2019), 107456.
[75] R. Stefanescu, G.D. Stanciu, A. Luca, L. Paduraru, B.I. Tamba, Secondary metabolites from plants possessing inhibitory properties against beta-amyloid aggregation as revealed by Thioflavin-T assay and correlations with investigations on transgenic mouse models of Alzheimer's disease, Biomolecules 10 (6) (2020) 870.
[76] S.L. Bernstein, N.F. Dupuis, N.D. Lazo, T. Wyttenbach, M.M. Condron, G. Bitan, D. B. Teplow, J.E. Shea, B.T. Ruotolo, C.V. Robinson, M.T. Bowers, Amyloid-beta protein oligomerization and the importance of tetramers and dodecamers in the aetiology of Alzheimer's disease, Nat. Chem. 1 (4) (2009) 326–331.
[77] W.A. Eimer, R. Vassar, Neuron loss in the 5XFAD mouse model of Alzheimer's disease correlates with intraneuronal Abeta42 accumulation and Caspase-3 activation, Mol. Neurodegener. 8 (2013) 2.
[78] N. Herrmann, S.A. Chau, I. Kircanski, K.L. Lanctot, Current and emerging drug treatment options for Alzheimer's disease: a systematic review, Drugs 71 (15) (2011) 2031–2065.
[79] R. Anand, K.D. Gill, A.A. Mahdi, Therapeutics of Alzheimer's disease: past, present and future, Neuropharmacology 76 Pt (2014) 27–50.
[80] K.I. Avgerinos, L. Ferrucci, D. Kapogiannis, Effects of monoclonal antibodies against amyloid-beta on clinical and biomarker outcomes and adverse event risks: a systematic review and meta-analysis of phase III RCTs in Alzheimer's disease, Ageing Res. Rev. 68 (2021), 101339.
[81] S. Mukhopadhyay, D. Banerjee, A primer on the evolution of Aducanumab: the first antibody approved for treatment of Alzheimer's disease, J. Alzheimers Dis. (2021).
[82] J. Cao, J. Hou, J. Ping, D. Cai, Advances in developing novel therapeutic strategies for Alzheimer's disease, Mol. Neurodegener. 13 (1) (2018) 64.
[83] E. Calzoni, A. Cesaretti, A. Polchi, A. Di Michele, B. Tancini, C. Emiliani, Biocompatible polymer nanoparticles for drug delivery applications in cancer and neurodegenerative disorder Therapies, J. Funct. Biomater. 10 (1) (2019).